

The Influence of Reaction-Induced Thermal Convection on the Electrical Currents Measured in Chronoamperometry and Cyclic Voltammetry

Javor Kirilov Novev, Shaltiel Eloul, and Richard G Compton

J. Phys. Chem. C, **Just Accepted Manuscript** • DOI: 10.1021/acs.jpcc.6b03413 • Publication Date (Web): 31 May 2016

Downloaded from <http://pubs.acs.org> on June 3, 2016

Just Accepted

"Just Accepted" manuscripts have been peer-reviewed and accepted for publication. They are posted online prior to technical editing, formatting for publication and author proofing. The American Chemical Society provides "Just Accepted" as a free service to the research community to expedite the dissemination of scientific material as soon as possible after acceptance. "Just Accepted" manuscripts appear in full in PDF format accompanied by an HTML abstract. "Just Accepted" manuscripts have been fully peer reviewed, but should not be considered the official version of record. They are accessible to all readers and citable by the Digital Object Identifier (DOI®). "Just Accepted" is an optional service offered to authors. Therefore, the "Just Accepted" Web site may not include all articles that will be published in the journal. After a manuscript is technically edited and formatted, it will be removed from the "Just Accepted" Web site and published as an ASAP article. Note that technical editing may introduce minor changes to the manuscript text and/or graphics which could affect content, and all legal disclaimers and ethical guidelines that apply to the journal pertain. ACS cannot be held responsible for errors or consequences arising from the use of information contained in these "Just Accepted" manuscripts.



The Influence of Reaction-Induced Thermal Convection on the Electrical Currents Measured in Chronoamperometry and Cyclic Voltammetry

Javor K. Novev, Shaltiel Eloul and Richard G. Compton*

Department of Chemistry, Physical and Theoretical Chemistry Laboratory, Oxford University,
South Parks Road, Oxford, OX1 3QZ, UK.

*Corresponding author. E-mail: Richard.Compton@chem.ox.ac.uk; Fax: +44 (0)1865 275 410; Tel: +44 (0)1865 275 957

Abstract: Electrochemical reactions invariably occur with a change in the molar volume between reactant and product, as well as a change in enthalpy. These factors give rise to convective flows driven respectively by concentration and temperature and affect the mass transport in the system, but the latter has received very little attention in the scientific literature. The present study attempts to fill this gap by quantifying the effect of thermal convection on the electrical currents in chronoamperometry and cyclic voltammetry, using the electrochemical oxidation of hexacyanoferrate (II) to hexacyanoferrate (III) as a model reaction. To this end, finite element numerical simulations of both electroanalytical techniques have been performed over a broad range of electrode radii (0.25 to 25 mm). The results presented here indicate that for chronoamperometry, convection has a substantial *overall* effect on the current, but *thermal* convection in particular is practically negligible for the studied systems. In contrast, for cyclic voltammetry performed under similar conditions, neither type of convection plays a significant role.

I. Introduction

Mass transport by natural convection can never be completely eliminated in electroanalytical experiments such as chronoamperometry, cyclic voltammetry and scanning electrochemical microscopy (SECM). However, modelling convective flows significantly complicates the interpretation of data from these techniques and they are rarely considered in the literature. While their importance can be minimised by employing low concentrations of the redox species, micro-sized electrodes and short experimental timescales¹, it has been recently demonstrated² that the validity of this approximation may be severely restricted in certain experimental configurations.

In contrast to the case of *forced* convection, where the flow is imposed by an external factor (as with the rotating disc electrode), *natural* convective flows are driven by buoyancy forces arising within the fluid. Depending on the driving force, we can distinguish between two types of natural convection – one is driven by concentration gradients

(solutal) and the other - by temperature gradients (thermal). Solutal convection unavoidably arises in the course of electrochemical processes – electrochemical reactions occur with a transfer of charge to or from the reacting species, which in turn leads to a change in its molar volume due to electrostriction³. The importance of solute-driven natural convection in electrochemical systems has been discussed for various systems, e.g. reactions occurring at vertical macroelectrodes in the work of Selman and Newman⁴ and cyclic voltammetry at macroelectrodes in the experimental study by Bond et al.⁵. Nevertheless, the effect of natural convection due to density gradients is usually neglected as it significantly complicates the analysis of experimental data. Gao et al.⁶ demonstrated that this is justified for microelectrodes and low analyte concentrations. However, according to a previous study by our group², natural convection is important even at analyte concentrations as low as 10 mM for electrode radii of the order of 0.1 mm or larger. Furthermore, as both Gao et al.⁶ and Ngamchuea et al.² show, the magnitude of the effect strongly depends on the orientation of the electrode.

Similarly, thermal convection in electrochemical systems is usually disregarded on the basis of the assumption that thermostating of the experimental cell eliminates all variations in temperature. Temperature variations caused by external factors, e.g. heating of the electrode, have been studied in the literature⁷. A study by Kamotani et al.⁸ dealt with the interplay between an externally imposed thermal convection and the solutal convection driven by an electrochemical reaction in a cell with vertical macroelectrodes. The temperature variations induced by the change of enthalpy of the electrochemical process itself, however, have not received much attention.

Our aim in the present study is to assess the importance of thermal convection driven by the intrinsic enthalpy change of an electrochemical process, thereby throwing light on a little studied but ubiquitous phenomenon. As we are interested in determining whether the effect can become important under any circumstances, we will only consider configurations that maximise it, e.g. by choosing the electrode orientation that yields the largest possible effect and assuming that all of the heat generated by the electrochemical reaction is dissipated in the solution. Since the main purpose of this study is to establish whether convective effects are important under these optimal conditions rather than to quantify them precisely, we will restrict our treatment to the main effects in the system and neglecting sources of additional complexity that do not lead to a qualitatively different behaviour. Effects that are present in our system, but not essential for its qualitative results, will be neglected, e.g., the finite size of the insulating sheath in real systems and the influence of the nonelectroactive species on the variation in the solution density. Following Ngamchuea et al.², we will use the well-studied redox couple hexacyanoferrate (III)/hexacyanoferrate (II) as a model system.

II. Theory

The first part of this section contains the mathematical equations that we use to describe the coupled thermal and solutal convection in electrochemical systems. In the second part, we give a description of the simulation procedures we use to solve these equations.

1. Model

1.A. Mass Transfer

A single-electron electrochemical oxidation is assumed to occur at the surface of an electrode,



The transfer of charge in reaction (1) means that it occurs with a change in molar volume due to the electrostrictive effect³. Furthermore, the reaction is accompanied by a change in enthalpy (ΔH), which means that, depending on the sign of ΔH , the electrode becomes either a heat source or a heat sink. Both factors generate local changes in the density of the solution, and therefore, buoyancy forces. The point of this study is to determine the effect of the temperature-driven natural convection on the electrical currents measured in chronoamperometrical or voltammetric experiments. To do that, we need to solve the convection-diffusion equation for the reduced species,

$$\frac{\partial C_{\text{Red}}}{\partial t} + \mathbf{v} \cdot \nabla C_{\text{Red}} = D_{\text{Red}} \nabla^2 C_{\text{Red}}. \quad (2)$$

where C_{Red} denotes the concentration of the reduced species, D_{Red} - its diffusion coefficient, t is time and \mathbf{v} stands for the velocity field. In eq. (2), we make the assumption that the system under consideration contains an excess of supporting electrolyte and, hence, the influence of migration on the mass transport of the electroactive species is negligible⁹⁻¹⁰. Eq. (2) also contains the approximation that the fluid is incompressible (see eq. (31)). For the small velocities that arise in our system, this makes the calculations considerably simpler without introducing a significant error¹¹.

In our treatment of the problem, we neglect the difference between the diffusion coefficients of the oxidised and the reduced species. This leads to the simplification

$$C_{\text{Red}} + C_{\text{Ox}} = C_{\text{bulk}}, \quad (3)$$

where C_{Ox} refers to the concentration of the oxidised species and C_{bulk} is the initial concentration of the reduced species (see eq. (4) below). The simple relationship between C_{Ox} and C_{Red} enables us to determine the concentrations of both species from the solution of eq. (2)⁹.

We model a finite cylindrical volume of radius r_{\max} and height z_{\max} , which makes it convenient to use cylindrical coordinates (r – radial, z – normal), shown schematically in Figure 1. Due to the symmetry of the problem, all studied quantities are independent of the polar angle ϕ . The coordinate origin is at the centre of the disc electrode of radius r_e . The direction of the z -axis is opposite to that of the gravitational force, i.e., the electrode is situated at the bottom of the electrochemical cell – as shown by Ngamchuea et al.², this configuration corresponds to a maximum effect of natural convection on the chronoamperometric current. The annular region surrounding the electrode ($z = 0$, $r_e < r < r_{\max}$) is made of a thermally and electrically insulating material and has a radius much larger than r_e .

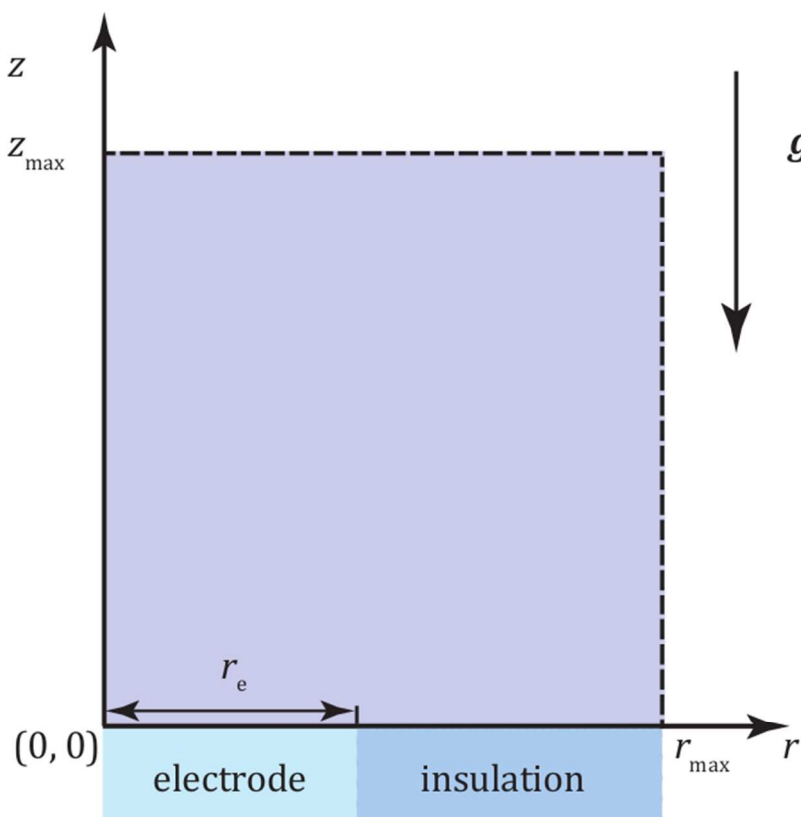


Figure 1. Schematic drawing of the simulated cell (not to scale). Because of the rotational symmetry of the problem, it is sufficient to solve the equations for a rectangular region of dimensions r_{\max} by z_{\max} . The coordinate origin is in the centre of the disc-shaped electrode of radius r_e . The annular region next to electrode, corresponding to $z = 0$ and $r_e < r < r_{\max}$, is thermally and electrically insulated, i.e. no flux passes through it. The vector of gravitational acceleration is $\mathbf{g} = -|g|\mathbf{e}_z$, where \mathbf{e}_z is the unit vector in the normal direction.

At the start of the process, $t = 0$, only the reduced species is present, and its concentration is assumed to be homogeneous and equal to C_{bulk} ,

$$C_{\text{Red}}(t = 0) = C_{\text{bulk}}. \quad (4)$$

At the boundaries of the simulated cell, the concentration is unperturbed from its initial bulk value,

$$C_{\text{Red}}(t, z = z_{\text{max}}) = C_{\text{bulk}}; \quad (5)$$

$$C_{\text{Red}}(t, r = r_{\text{max}}) = C_{\text{bulk}}. \quad (6)$$

Employing a boundary condition for the flux instead of the concentration at $r = r_{\text{max}}$ makes it easier to obtain an accurate numerical solution of the problem⁹. For that reason, the simulations were performed with

$$\left. \frac{\partial C_{\text{Red}}}{\partial r} \right|_{t, r=r_{\text{max}}} = 0 \quad (7)$$

instead of eq. (6). The dimensions of the simulated region of space, r_{max} and z_{max} , are chosen in such a way as to guarantee that none of the properties of the solution are perturbed at the edges of the cell. At $r_e \sim 1$ cm or below, the perturbation in temperature spreads furthest (see Figures 8-9 in Section III below) to distances of the order of $L_{\text{therm}} \sim \sqrt{t_{\text{max}}\chi}$, where t_{max} is the duration of the simulated experiment and χ [$\text{m}^2\cdot\text{s}^{-1}$] is the thermal diffusivity of the fluid. For that reason, simulations of electrodes of $r_e < 1$ cm were performed with $r_{\text{max}} = r_e + 6\sqrt{t_{\text{max}}\chi}$ and $z_{\text{max}} = 6\sqrt{t_{\text{max}}\chi}$. For $r_e > 1$ cm, the perturbations in the fluid velocity have the largest spatial extent, $L_{\text{hydr}} \sim r_e$ (see Figure 9 below), and the dimensions of the cell were chosen to be $r_{\text{max}} = z_{\text{max}} = 4 \cdot r_e$. The concentration profile needs to be symmetric around $r = 0$, i.e.

$$\left. \frac{\partial C_{\text{Red}}}{\partial r} \right|_{r=0} = 0. \quad (8)$$

Assuming that the electrode kinetics of the reaction (1) are fast in relation to the rate of mass transport, we can write a Nernstian boundary condition for the concentration of the reduced species at the electrode surface⁹:

$$C_{\text{Red}}|_{r \leq r_e, z=0} = \frac{C_{\text{bulk}}}{1 + \exp\left[\frac{F(E - E_f^0)}{RT}\right]}, \quad (9)$$

where $F = 96485.332 \text{ C}\cdot\text{mol}^{-1}$ is the Faraday constant, $R = 8.31445 \text{ J}\cdot\text{mol}^{-1}\cdot\text{K}^{-1}$ is the gas constant, E is the electrode potential and E_f^0 is the formal potential of the redox couple Ox/Red. The insulating surface acts as a reflecting boundary and therefore, there must be no normal flux through it:

$$\left. \frac{\partial C_{\text{Red}}}{\partial z} \right|_{z=0, r_e \leq r \leq r_{\text{max}}} = 0. \quad (10)$$

The electrical current density i is proportional to the mass flux at $z = 0$,

$$i = FD_{\text{red}} \left. \frac{\partial C_{\text{Red}}}{\partial z} \right|_{z=0}. \quad (11)$$

The total electrical current (I) is obtained by integrating eq. (11) over the electrode surface:

$$I = 2\pi \int_0^{r_e} i r dr. \quad (12)$$

1.B. Heat Transfer

The heat transfer in the system is coupled to the mass transport and to determine the concentration profile explicitly, we also need to solve the convective heat transfer equation,

$$\frac{\partial T}{\partial t} + \mathbf{v} \cdot \nabla T = \chi \nabla^2 T, \quad (13)$$

where T is the temperature of the fluid. The boundary conditions for T at the edge of the cell, the initial condition and the symmetry condition are analogous to (4)-(8) for C_{Red} ,

$$T(t = 0) = T_{\text{bulk}}; \quad (14)$$

$$T(t, z = z_{\text{max}}) = T_{\text{bulk}}; \quad (15)$$

$$T(t, r = r_{\text{max}}) = T_{\text{bulk}}; \quad (16)$$

$$\left. \frac{\partial T}{\partial r} \right|_{r=0} = 0. \quad (17)$$

As with the mass transport problem, it is more computationally effective to employ a Neumann boundary condition instead of eq. (16):

$$\left. \frac{\partial T}{\partial r} \right|_{t, r=r_{\text{max}}} = 0. \quad (18)$$

As the cell dimensions are large enough to guarantee that the temperature at its edges remains unchanged, eq. (15) can also be replaced with a Neumann boundary condition,

$$\left. \frac{\partial T}{\partial z} \right|_{t, z=z_{\text{max}}} = 0. \quad (19)$$

Due to the thermal insulation, the heat flux through $z = 0$ is zero at $r > r_e$,

$$\left. \frac{\partial T}{\partial z} \right|_{z=0, r_e \leq r \leq r_{\text{max}}} = 0. \quad (20)$$

The reaction occurs with a change in enthalpy, which gives rise to a heat flux at the electrode surface. In the Nernstian limit, neglecting ohmic losses, the normal heat flux is proportional to the normal mass flux¹²:

$$q(z = 0) = -\Delta H \cdot D_{\text{Red}} \left. \frac{\partial C_{\text{Red}}}{\partial z} \right|_{z=0}. \quad (21)$$

On the other hand, from Fourier's law, the heat flux can also be expressed through the temperature gradient:

$$q(z = 0) = -\kappa \left. \frac{\partial T}{\partial z} \right|_{z=0}, \quad (22)$$

where κ [$\text{W}\cdot\text{m}^{-1}\cdot\text{K}^{-1}$] is the thermal conductivity of the fluid, $\kappa = \rho\chi c_p$, with c_p being the specific heat capacity in $\text{J}\cdot\text{kg}^{-1}\cdot\text{K}^{-1}$.

In general, the enthalpy of the reaction is a function of concentration. From the definitions of the enthalpy and the Gibbs energy it follows that under isothermal conditions for the overall process

$$\Delta H = \Delta G + T\Delta S. \quad (23)$$

At equilibrium, $\Delta G = 0$, which leaves

$$\begin{aligned} \Delta H &= T\Delta S = T(\Delta S_{\text{reaction}} + \Delta S_{\text{migration}}) = T\left(-\frac{\partial \Delta G_{\text{reaction}}}{\partial T} + \Delta S_{\text{migration}}\right) \\ &= T\left(F\frac{\partial E}{\partial T} + \Delta S_{\text{migration}}\right) \\ &= FT\frac{\partial}{\partial T}\left(E_f^0 + \frac{RT}{F}\ln\frac{a_{\text{Ox}}}{a_{\text{Red}}}\right) + T\Delta S_{\text{migration}}, \end{aligned} \quad (24)$$

where $\Delta S_{\text{reaction}}$ and $\Delta G_{\text{reaction}}$ are respectively the change in entropy and Gibbs energy change intrinsic to reaction (1) and a_i is the activity of species i . we used the definition of the electrode potential and the Nernst equation. The activities of the oxidised and reduced species and their derivatives with respect to temperature depend on the concentrations of the reduced and oxidised species, as well as that of the supporting electrolyte. The term $T\Delta S_{\text{migration}}$ accounts for the heat of transport of the non-electroactive ions in the solution¹³ and is also dependent upon the concentration of the supporting electrolyte. However, as we are mostly interested in the qualitative effect of temperature-induced free convection, we will treat ΔH as a constant. For our simulations, we will use the value of $45.35 \text{ kJ}\cdot\text{mol}^{-1}$ measured by Boudeville and Tallec¹² for $0.1 \text{ M } [\text{Fe}(\text{CN})_6]^{3-}/0.1 \text{ M } [\text{Fe}(\text{CN})_6]^{4-}$, which is in close agreement with the value of the standard enthalpy of $45.62 \text{ kJ}\cdot\text{mol}^{-1}$ that Fang et al.¹⁴ obtained by extrapolating their data for ΔH to infinite dilution of the reacting species.

Eqs. (21) and (22) enable us to assess the order of magnitude of the temperature change caused by the reaction. From dimensional analysis, the order of magnitude of $\partial T/\partial z$ is $\Delta T/L_{\text{therm}}$, where L_{therm} is the characteristic length of the thermal boundary layer and $\Delta T = T(z = 0) - T(z = L_{\text{therm}})$ is the change in temperature over that distance. Similarly, $\partial C_{\text{Red}}/\partial z \sim \Delta C_{\text{Red}}/L_{\text{diff}}$. Inserting those results in eqs. (21) and (22) and equating the right-hand sides, we obtain

$$\Delta T \sim -\Delta H \Delta C_{\text{Red}} \frac{D_{\text{Red}}}{\kappa} \frac{L_{\text{therm}}}{L_{\text{diff}}}. \quad (25)$$

For convection-free mass and heat transport, $L_{\text{diff}} = \sqrt{D_{\text{Red}} t}$ and $L_{\text{therm}} = \sqrt{\chi t}$. In the cases studied here, the inclusion of convection has no effect on the order of magnitude of L_{diff} and L_{therm} , which enables us to rewrite eq. (25) as

$$\Delta T \sim -\Delta H \Delta C_{\text{Red}} \frac{D_{\text{Red}}}{\kappa} \sqrt{\frac{\chi}{D_{\text{Red}}}} = -\Delta H \Delta C_{\text{Red}} \frac{D_{\text{Red}}}{\kappa} \sqrt{\frac{\kappa}{\rho c_p D_{\text{Red}}}} = -\Delta H \Delta C_{\text{Red}} \sqrt{\frac{D_{\text{Red}}}{\rho c_p \kappa}}. \quad (26)$$

1.C. Hydrodynamics

To determine the velocity of the fluid, which appears in eqs. (2) and (13), we need to solve the Navier-Stokes equation for an incompressible viscous fluid,

$$\rho \left(\frac{\partial \mathbf{v}}{\partial t} + \mathbf{v} \cdot \nabla \mathbf{v} \right) = -\nabla p + \eta \nabla^2 \mathbf{v} + \rho \mathbf{g}, \quad (27)$$

where ρ is the solution density, η is its viscosity, p is the pressure and \mathbf{g} is the gravitational acceleration.

The Navier-Stokes equation must be solved together with the continuity equation, which for an incompressible fluid has the form

$$\nabla \cdot \mathbf{v} = 0. \quad (28)$$

The fluid is at rest at the start of the simulated experiment, $t = 0$,

$$\mathbf{v}(t = 0) = \mathbf{0}. \quad (29)$$

The velocity of the bulk solution is assumed to be unperturbed,

$$\mathbf{v}|_{r=r_{\text{max}}} = \mathbf{v}|_{z=z_{\text{max}}} = \mathbf{0}. \quad (30)$$

A no-slip boundary condition is applied to the solid surface at $z = 0$,

$$\mathbf{v}|_{z=0} = \mathbf{0}. \quad (31)$$

Symmetry boundary conditions are employed at the cylinder axis,

$$v_r|_{r=0} = 0; \quad (32)$$

$$\left. \frac{\partial v_z}{\partial r} \right|_{r=0} = \left. \frac{\partial v_r}{\partial z} \right|_{r=0} = 0. \quad (33)$$

Equations (32)-(33) are equivalent to eqs. 1.3-1.4 in Demkowicz's paper for a system with plane symmetry¹⁵.

The chemical reaction (1) affects the solution density in two ways – through the formation of a product which differs in molar volume from the reactant as well as through variations in the temperature of the solution caused by heat flux (22). Assuming both

effects lead to small perturbations, we can approximate the density ρ with its first-order Taylor expansion,

$$\rho \approx \rho_0 + \left(\frac{\partial \rho}{\partial C_{\text{Red}}} \right)_{T,p} (C_{\text{Red}} - C_{\text{bulk}}) + \left(\frac{\partial \rho}{\partial T} \right)_{p,C_{\text{Red}}} (T - T_{\text{bulk}}) \approx \rho_0 [1 + \beta(C_{\text{bulk}} - C_{\text{Red}}) - \alpha(T - T_{\text{bulk}})], \quad (34)$$

where ρ_0 is the density of the unperturbed solution, β [$\text{m}^3 \cdot \text{mol}^{-1}$] is the densification coefficient for the specific reaction and $\alpha = -1/\rho_0 \cdot (\partial \rho_0 / \partial T)_{p,C_{\text{Red}}} [\text{K}^{-1}]$ is the thermal expansion coefficient of the initial solution. In eq. (34), we have used that at constant temperature the density of the solution can be expressed through the concentrations of the ionic species present and their individual densification coefficients⁴, (β_i),

$$\rho - \rho_0 = \sum_i \beta_i (C_i - C_i(t=0)). \quad (35)$$

It should be noted that the sum in eq. (35) is over all species and the coefficients β_i are defined for each individual ion, in contrast to the definition used by Selman and Newman⁴. Assuming that the concentrations of the nonelectroactive species are unperturbed and using the approximate mass balance (3), we obtain the concentration-dependent term from (34) with $\beta = \beta_{\text{Ox}} - \beta_{\text{Red}}$. The change in density in a two-component mixture with a solute of concentration C , molar mass M and molar volume v is¹⁶ $\rho - \rho_s = (M - \rho_s v)C$, where for dilute solutions v can be regarded as a constant and ρ_s is the density of the pure solvent. For an arbitrary number of components, this generalises to¹⁷

$$\rho - \rho_s = \sum_i (M_i - \rho_s v_i) C_i. \quad (36)$$

Substituting eq. (36) in eq. (35), we obtain the equation

$$\rho - \rho_0 = \sum_i (M_i - \rho_s v_i) (C_i - C_i(t=0)), \quad (37)$$

from which it is apparent that $\beta_i = M_i / \rho_s - v_i$. As our system contains KNO_3 as a supporting electrolyte, eq. (37) includes contributions from four types of ions ($[\text{Fe}(\text{CN})_6]^{4-}$, $[\text{Fe}(\text{CN})_6]^{3-}$, K^+ , NO_3^-). However, as we are mainly interested in the qualitative effect of convection on the mass transport, we will only consider the leading term, i.e., the contribution of the electroactive ions. As we work under the approximation that the diffusion coefficients of the reduced and oxidised are equal, we can use (3) to reach

$$\rho - \rho_0 \approx (\beta_{\text{Ox}} - \beta_{\text{Red}})(C_{\text{bulk}} - C_{\text{Red}}) = (v_{\text{Red}} - v_{\text{Ox}})(C_{\text{bulk}} - C_{\text{Red}}). \quad (38)$$

We can follow the approach employed by Feldberg and Lewis¹⁷ to estimate the effect of the supporting electrolyte on the solution density. Using the condition for local

electroneutrality and the approximation that the diffusion coefficients of *all* present species are equal, we can estimate that including the contribution of the supporting electrolyte would lead to the expression

$$\rho - \rho_0 = \left(\beta_{\text{Ox}} - \beta_{\text{Red}} + \frac{\beta_{\text{NO}_3^-} - \beta_{\text{K}^+}}{2} \right) (C_{\text{bulk}} - C_{\text{Red}}). \quad (39)$$

Using literature data for the individual ionic molar volumes¹⁸, we can quantify the term due to the supporting electrolyte:

$$\frac{1}{2} (\beta_{\text{NO}_3^-} - \beta_{\text{K}^+}) = \frac{1}{2} \left(\frac{M_{\text{NO}_3^-} - M_{\text{K}^+}}{\rho_s} + v_{\text{K}^+} - v_{\text{NO}_3^-} \right) = -0.397 \times 10^{-5} \text{ m}^3 \cdot \text{mol}, \quad (40)$$

while $\beta_{\text{Ox}} - \beta_{\text{Red}} = v_{\text{Red}} - v_{\text{Ox}} = -4.13 \times 10^{-5} \text{ m}^3 \cdot \text{mol}$, i.e., the effect of the supporting electrolyte on the solution density is one order of magnitude weaker than that of the electroactive species. Thus, as we are more interested in the qualitative effect of natural convection than its precise quantification, we employ eq. (38) for all our calculations.

It is more convenient to rewrite the Navier-Stokes equation in terms of the difference in pressure with respect to the initial state instead of the absolute pressure,

$$\Delta p = p - p_0 + \rho z |g|, \quad (41)$$

where p_0 is the pressure at $z = 0$. The initial condition for Δp is that

$$\Delta p|_{t=0} = 0. \quad (42)$$

Substituting eqs. (34)-(41) in eq. (27) and neglecting terms of second or higher order leads to a modified form of the Navier-Stokes equation¹⁹,

$$\rho_0 \left(\frac{\partial \mathbf{v}}{\partial t} + \mathbf{v} \cdot \nabla \mathbf{v} \right) = -\nabla \Delta p + \eta \nabla^2 \mathbf{v} + \mathbf{F}_b, \quad (43)$$

in which \mathbf{F}_b is the buoyancy force generated by the chemical reaction,

$$\mathbf{F}_b = (\rho - \rho_0) \mathbf{g} = \rho_0 [\beta (C_{\text{bulk}} - C_{\text{Red}}) - \alpha (T - T_{\text{bulk}})] \mathbf{g}. \quad (44)$$

The upper limit for \mathbf{F}_b is its value in the vicinity of the electrode, where the perturbations in concentration and temperature originate. Therefore, we can substitute $T - T_{\text{bulk}}$ with ΔT from eq. (26), to obtain an assessment of the order of magnitude of the buoyancy force:

$$\begin{aligned} \mathbf{F}_b &= (\rho - \rho_0) \mathbf{g} \sim \rho_0 \beta \Delta C_{\text{Red}} \left[1 + \Delta H \frac{\alpha}{\beta} \frac{D_{\text{Red}}}{\kappa} \frac{L_{\text{therm}}}{L_{\text{diff}}} \right] \mathbf{g} \approx \\ &\rho_0 \left[\beta \Delta C_{\text{Red}} + \alpha \Delta H \Delta C_{\text{Red}} \sqrt{\frac{D_{\text{Red}}}{\rho c_p \kappa}} \right] \mathbf{g} = \rho_0 \beta \Delta C_{\text{Red}} \left[1 + \Delta H \frac{\alpha}{\beta} \sqrt{\frac{D_{\text{Red}}}{\rho c_p \kappa}} \right] \mathbf{g}. \end{aligned} \quad (45)$$

Our model reaction, the oxidation of hexacyanoferrate (II) to hexacyanoferrate (III), has a negative densification coefficient β , which means that the buoyancy force \mathbf{F}_b opposes

the gravitational force. Ngamchuea et al.² have shown that in this case, the solutal convection is most intense if the electrode is placed in the bottom of the cell, which is the reason we model that particular configuration.

Thermal convection can either oppose or reinforce solutal convection and as we see from eq. (45), this depends on the sign of the ratio between the densification coefficient (β) and the enthalpy of the reaction (ΔH). For our model reaction, $\Delta H/\beta < 0$, i.e., thermal convection counteracts solutal convection. Nevertheless, to test qualitatively the relative importance of thermal convection, we performed simulations with $\Delta H/\beta > 0$, in which the sign of ΔH was reversed, both with the actual absolute value of the enthalpy and with a magnitude increased several times. This can be achieved in practice for an irreversible endothermic process by applying a sufficiently high overpotential, see eq. 2.9 in Vetter's book²⁰.

The dimensionless quantity $N = \alpha \left| \frac{\Delta H}{\beta} \right| \sqrt{\frac{D_{\text{Red}}}{\rho c_p \kappa}}$ in eq. (45) reflects the ratio between the buoyancy forces caused by the variation in temperature and density. N is equivalent to the buoyancy ratio defined by Pringle and Glass in their treatment of a similar problem that involves coupled heat and mass transfer²¹. It can also be interpreted as the ratio of the Rayleigh numbers for natural convection driven by gradients in temperature and concentration, as in the work of Singh and Srinivasan²². Substituting the characteristic numerical values for our problem, we can estimate its order of magnitude:

$$N = \alpha \left| \frac{\Delta H}{\beta} \right| \sqrt{\frac{D_{\text{Red}}}{\rho c_p \kappa}} = \frac{2.06 \times 10^{-4} \times 4.53 \times 10^4}{4.13 \times 10^{-5}} \sqrt{\frac{7.53 \times 10^{-10}}{998 \times 4182 \times 0.5984}} = 3.93 \times 10^{-3}. \quad (46)$$

The parameters of the solution were approximated by their values for pure water, $\alpha = 2.06 \times 10^{-4} \text{ K}^{-1}$, $\kappa = 0.5984 \text{ W} \cdot \text{m}^{-1} \cdot \text{K}^{-1}$, $\rho = 998 \text{ kg} \cdot \text{m}^{-3}$ and $c_p = 4181.8 \text{ J} \cdot \text{kg}^{-1} \cdot \text{K}^{-1}$ at 293.15 K, taken from the CRC Handbook of Chemistry and Physics²³; the densification coefficient of the oxidation of hexacyanoferrate (II) to hexacyanoferrate (III), $\beta = \beta_{\text{Ox}} - \beta_{\text{Red}} = v_{\text{Red}} - v_{\text{Ox}} = -4.13 \times 10^{-5} \text{ m}^3 \cdot \text{mol}^{-1}$, was calculated from the data tabulated by Marcus¹⁸ and its enthalpy change, $\Delta H = 45.35 \text{ kJ} \cdot \text{mol}^{-1}$, was taken from Boudeville and Tallec¹²; the diffusion coefficient of both species was taken to be equal to its value at $T = 298.15 \text{ K}$, $D_{\text{Red}} = 7.53 \times 10^{-10} \text{ m}^2 \cdot \text{s}^{-1}$, as determined by Ngamchuea et al.²⁵. The fact that $N \sim 10^{-3}$ means that the buoyancy force caused by temperature fluctuations is negligible for the oxidation of hexacyanoferrate (II) to hexacyanoferrate (III). Moreover, it seems unlikely that it will be important for any type of reaction in the problem we consider, as this would require a variation of orders of magnitude in ΔH or β . This conclusion is supported by the results from our simulations, as described below.

2. Simulations

Simulations of chronoamperometry and cyclic voltammetry were performed with the finite element package COMSOL Multiphysics 5.2²⁴.

The values of α , β , κ , c_p and D_{Red} given in Section II.1 were used for all simulations. The duration of all simulated experiments was $t_{\text{max}} = 60$ s; the formal potential $E_f^0 = 0.358$ V of the couple $[\text{Fe}(\text{CN})_6]^{3-}/[\text{Fe}(\text{CN})_6]^{4-}$ at 298.15 K. The simulations were performed with values of the viscosity and the density corresponding to 0.509 M KNO_3 as a supporting electrolyte at 293.15 K²³ – $\eta = 0.980$ mPa.s, $\rho_0 = 1029.8$ kg·m⁻³. The initial concentration of $[\text{Fe}(\text{CN})_6]^{4-}$ was set to the value used by Ngamchuea et al.², $C_{\text{bulk}} = 9.5$ mM. It should be noted that in the governing equations of the system, eqs. (2), (13) and (43), we have used the approximation that none of the properties of the solution except for the density depend on temperature, which is justified for the small variations of T that we consider (for a detailed analysis of a similar problem, see the paper by Gray and Giorgini²⁶). As $(T - T_{\text{bulk}})/T_{\text{bulk}} \ll 1$, we neglect the variation in temperature everywhere except in the heat transfer equation (13) and the buoyancy force (44) in the Navier-Stokes equation.

Three spatial configurations were used for the simulations:

- 1) electrode radius $r_e = 0.25$ mm and cell dimensions $r_{\text{max}} = r_e + 6\sqrt{t_{\text{max}}\kappa/(\rho_0 c_p)} = 17.58$ mm mm by $z_{\text{max}} = 17.33$ mm; 2) $r_e = 2.5$ mm, $r_{\text{max}} = r_e + 6\sqrt{t_{\text{max}}\kappa/(\rho_0 c_p)} = 19.82$ mm and $z_{\text{max}} = 6\sqrt{t_{\text{max}}\kappa/(\rho_0 c_p)} = 17.33$ mm; 3) $r_e = 25$ mm, $r_{\text{max}} = 4r_e = 100$ mm and $z_{\text{max}} = 4r_e = 100$ mm.

Three types of simulations were run for each electrode radius.

- 1) Diffusion-only – with a velocity field set to $\mathbf{v} = \mathbf{0}$ and no account for convection.
- 2) Diffusion coupled with solutal convection but no variations in temperature, corresponding to the simulations performed by Ngamchuea et al.².
- 3) Diffusion coupled with both solutal and thermal convection. Three values were used for the reaction enthalpy – a) the experimental value measured by Boudeville and Tallec²⁷, $\Delta H = 45.35$ kJ·mol⁻¹, b) its reverse and c) a limiting value of -100 kJ·mol⁻¹. The purpose of simulating case c) was to increase the effect of thermal convection to its reasonable limits and judge its relative importance.

For chronoamperometry, the applied electrode potential was $E_{\text{chrono}} = 0.863$ V, corresponding to a dimensionless potential $\theta = F(E - E_f^0)/(RT) = 20$ and a surface concentration of the reduced species $C_{\text{Red}}(r \leq r_e, z = 0) \sim 10^{-8}$ mol·m⁻³.

For the simulations of cyclic voltammetry, the electrode potential was varied according to the equation

$$E = \begin{cases} E_i + vt, t < t_{\max}/2 \\ 2E_v - E_i - vt, t \geq t_{\max}/2 \end{cases} \quad (47)$$

where $E_i = -0.147$ V is the potential at the start of the scan, $E_v = 0.863$ V is its value at the vertex (corresponding to -20 and 20 in θ) and the scan rate is $v = 2(E_v - E_i)/t_{\max} = 33.6 \text{ mV} \cdot \text{s}^{-1}$.

The spatial and the temporal discretisation of the problems were chosen in such a way that the simulations gave results that were sufficiently close to the exact expressions for the convection-free case. Linear shape functions were used for C_{Red} , T , Δp and v for every simulation except those of chronoamperometric experiments at $r_e = 0.25$ mm. In the latter case, cubic elements were employed for the concentration and linear for the other unknown functions.

For chronoamperometric simulations, the calculated current was compared to that predicted by the Shoup-Szabo equation²⁷,

$$I = 4\pi F D_{\text{Red}} r_e C_{\text{bulk}} \left[0.7854 + 0.4431 \frac{r_e}{\sqrt{D_{\text{Red}} t}} + 0.2146 \cdot \exp\left(-0.7823 \frac{r_e}{2\sqrt{D_{\text{Red}} t}}\right) \right], \quad (48)$$

and all simulations were performed with settings for the discretisation that guaranteed agreement to within 1% with eq. (48) at $t > 15$ s for the diffusion-only problem (see Figures 3, 5 and 7). At $t < 0.01$ s, the simulated currents for all cases exhibited considerable oscillations caused by the singularity of the current at $t \rightarrow 0$. At $0.01 \text{ s} < t < 15 \text{ s}$, the relative deviation of the convection-free simulation from eq. (48) goes through a peak value of approximately 3 %. As convection only starts to have an appreciable effect at $t \gg 15$ s (see Figures 2-7, compare with Figure 5 in the work of Ngamchuea et al.²), we disregard this initial period.

The height of the forward peak for the diffusion-only case was used as a criterion for the accuracy for simulations of cyclic voltammetry. The simulated peak height was compared to the one calculated from the following empirical equation²⁸:

$$I_{\max} = 4\pi F D_{\text{Red}} r_e C_{\text{bulk}} \left(0.34e^{-0.66\sqrt{\sigma}} + 0.66 - 0.13e^{-\frac{11}{\sqrt{\sigma}}} + 0.351\sqrt{\sigma} \right), \quad (49)$$

in which σ is the dimensionless scan rate, $\sigma = Fr_e^2 v / (RTD_{\text{Red}})$. The mesh and the time-stepping were chosen so that the difference between eq. (49) and the simulated peak current was within 1 % for the convection-free case. The same configuration yielded only an approximately correct result for the peak-to-peak separation, $\Delta E_{\text{pp}} = 2.218RT/F$ for reversible cyclic voltammetry with diffusion as the sole mode of mass transport⁹.

The theoretical midpoint potential for the convection-free case is equal to the formal potential²⁸,

$$E_{\text{mid}} = \frac{E(I_{\max}) + E(I_{\min})}{2} = E_f^0. \quad (50)$$

The time-stepping scheme for the problem determines the set of values of E for which the equations are solved through eq. (47). Our choice of time-stepping gives a result for E_{mid} that is accurate within 1 % for the diffusion-only problem, but is comparatively insensitive to changes in E_{mid} due to the relatively large interval between two consecutive values of E in the simulation.

III. Results and discussion

This section presents the results obtained from the simulations of chronoamperometry and cyclic voltammetry described in Section II.

1. Chronoamperometry

The currents obtained from the simulation setups described in Section II. 2 are plotted in Figures 2, 4 and 6 for $r_e = 0.25$, 2.5 and 25 mm, respectively. The relative difference between the simulated and the Shoup-Szabo current is plotted in Figures 3, 5 and 7. Figures 8 and 9 show ‘snapshots’ of C , T and \mathbf{v} from simulations that include both types of convection performed with the experimentally measured enthalpy of the modelled reaction at $r_e = 0.25$ mm and 25 mm respectively.

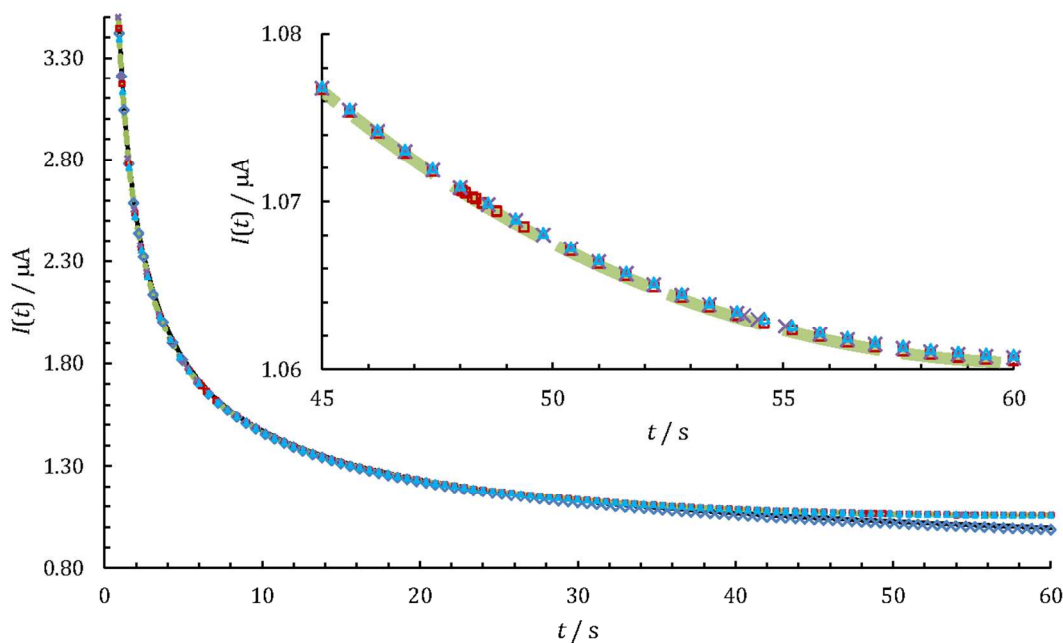


Figure 2. Dependence of current on time at $r_e = 0.25$ mm for various simulation setups plotted together with the Shoup-Szabo current (solid line). Legend as follows: diamonds – diffusion-only simulation; squares – simulation with convection driven by concentration gradients; dashed line – simulation with convection driven by concentration and temperature gradients with $\Delta H = 45.35$ kJ·mol⁻¹; crosses – simulation with both types of convection $\Delta H = -45.35$ kJ·mol⁻¹; triangles – simulation with both types of convection, $\Delta H = -100.0$ kJ·mol⁻¹. The inset shows the current for the various simulations that involve convection zoomed in for long times. For all simulations, $r_{\text{max}} = r_e + 6\sqrt{t_{\text{max}}\kappa/(\rho_0 c_p)} = 17.58$ mm and $z_{\text{max}} = 6\sqrt{t_{\text{max}}\kappa/(\rho_0 c_p)} = 17.33$ mm.

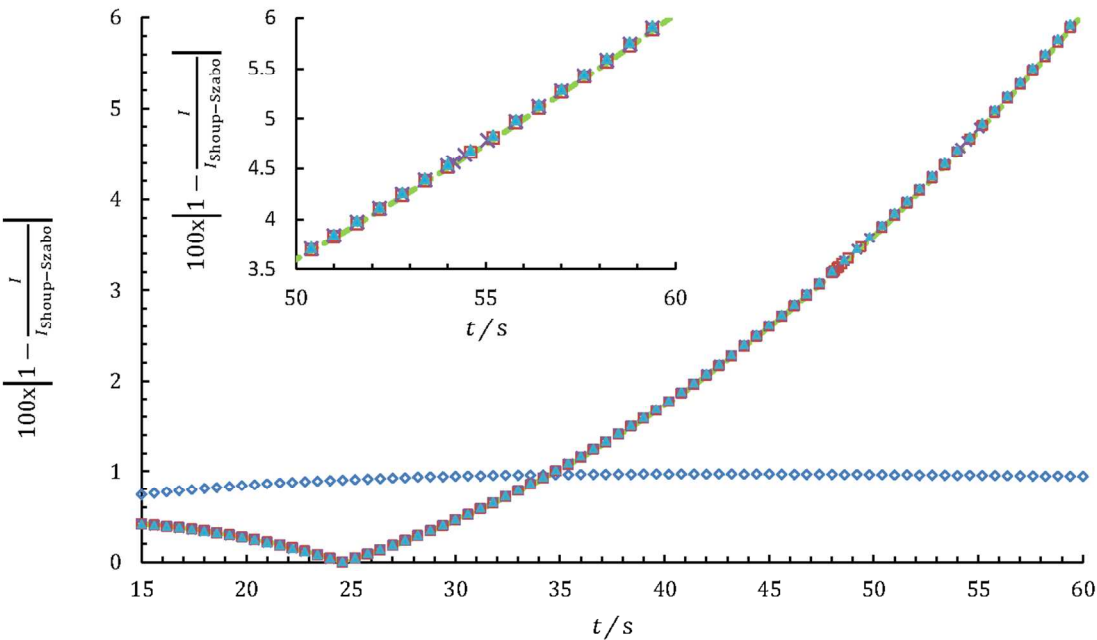


Figure 3. Relative difference between the currents obtained from various simulations and the Shoup-Szabo current at $r_e = 0.25$ mm. (legend as in Figure 2). The inset shows the current for the various simulations that involve convection zoomed in for long times. For all simulations, $r_{\text{max}} = r_e + 6\sqrt{t_{\text{max}}\kappa/(\rho_0 c_p)} = 17.58$ mm and $z_{\text{max}} = 6\sqrt{t_{\text{max}}\kappa/(\rho_0 c_p)} = 17.3$ mm.

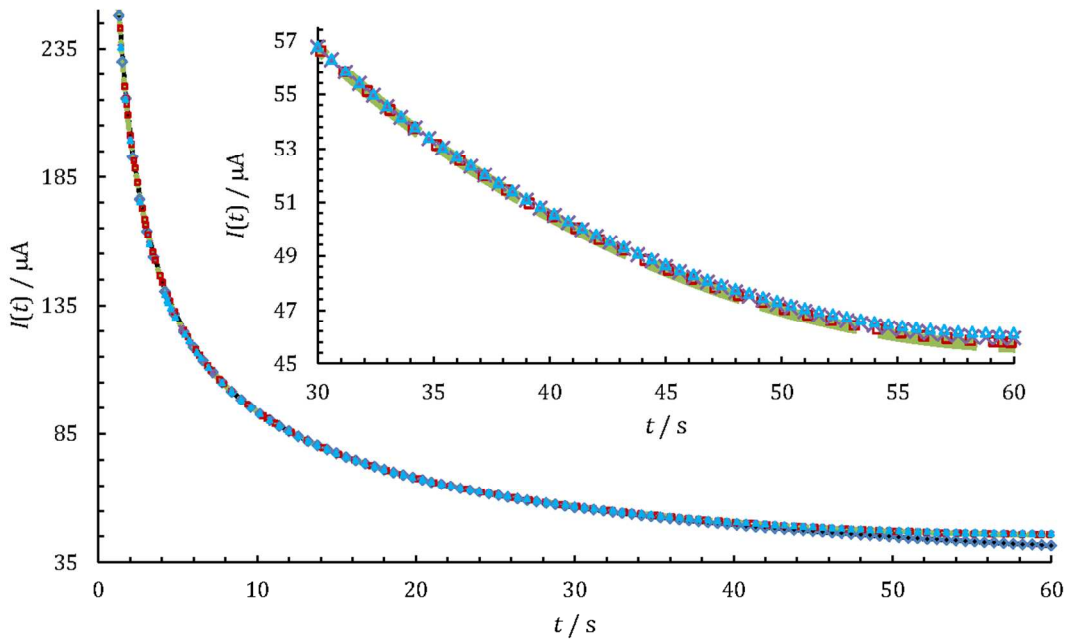


Figure 4. Dependence of current on time for various simulation setups at $r_e = 2.5$ mm plotted together with the Shoup-Szabo current (solid line, legend as in Figure 2). The inset shows the current for the various simulations that involve convection zoomed in for long times. For all simulations, $r_{\text{max}} = r_e + 6\sqrt{t_{\text{max}}\kappa/(\rho_0 c_p)} = 19.82$ mm and $z_{\text{max}} = 6\sqrt{t_{\text{max}}\kappa/(\rho_0 c_p)} = 17.33$ mm.

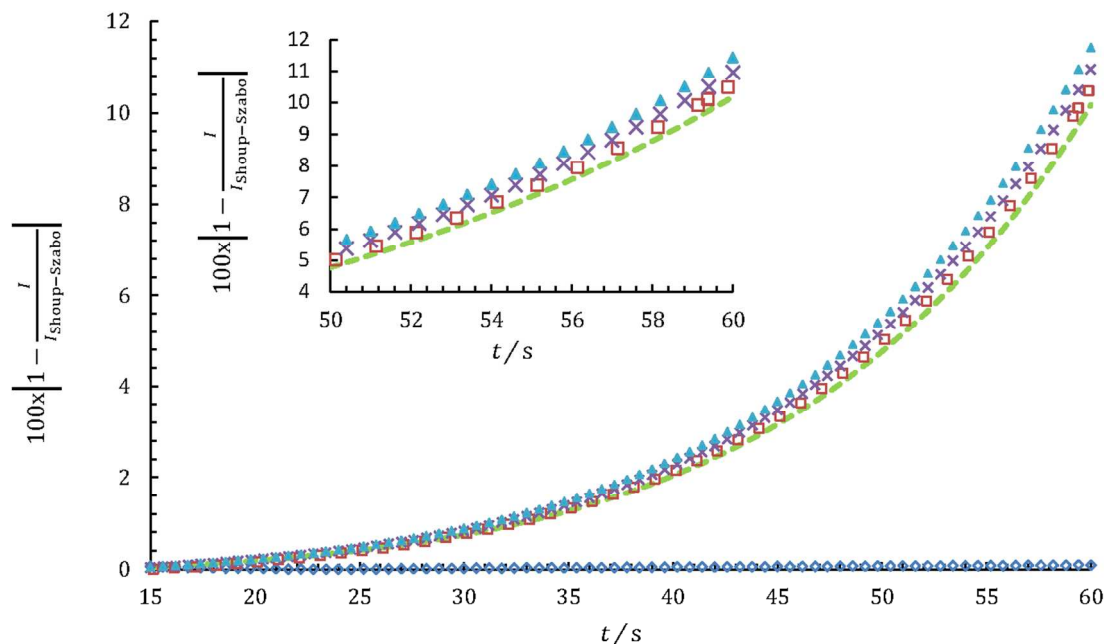


Figure 5. Relative deviation of the currents obtained from various simulations at $r_e = 2.5$ mm from the Shoup-Szabo current (legend as in Figure 2). The inset shows the current for the various simulations that involve convection zoomed in for long times. For all simulations, $r_{\max} = r_e + 6\sqrt{t_{\max}\kappa/(\rho_0 c_p)} = 19.82$ mm and $z_{\max} = 6\sqrt{t_{\max}\kappa/(\rho_0 c_p)} = 17.33$ mm.

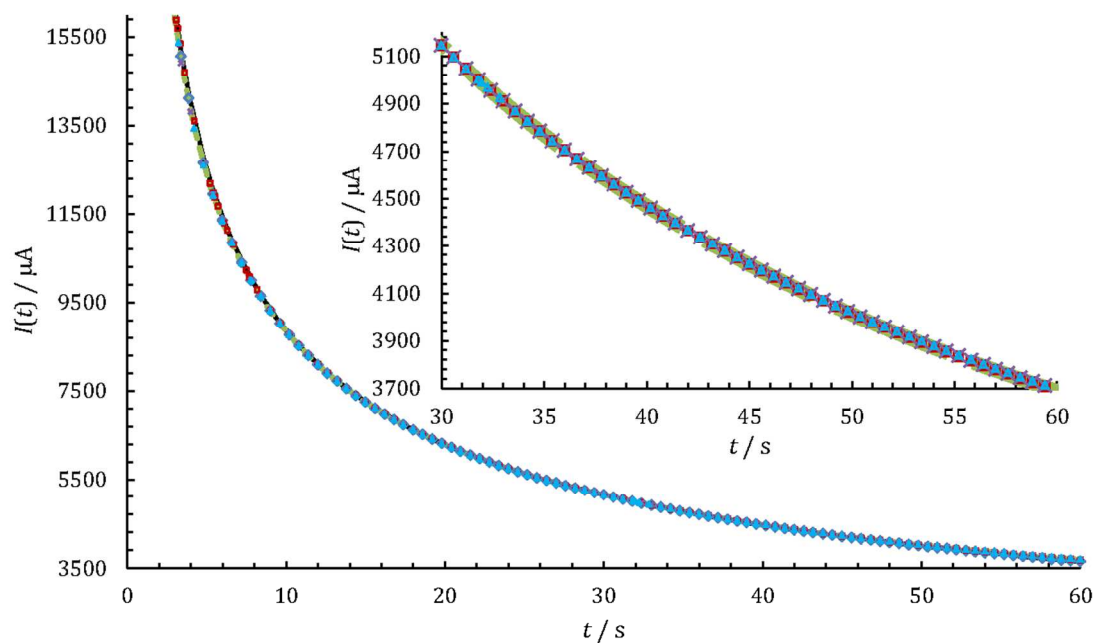


Figure 6. Dependence of current on time for various simulation setups plotted together with the Shoup-Szabo current (solid line, legend as in Figure 2) for an electrode of radius $r_e = 25$ mm. The inset shows the current for the various simulations that involve convection zoomed in for long times. For all simulations, $r_{\max} = z_{\max} = 4r_e = 100$ mm.

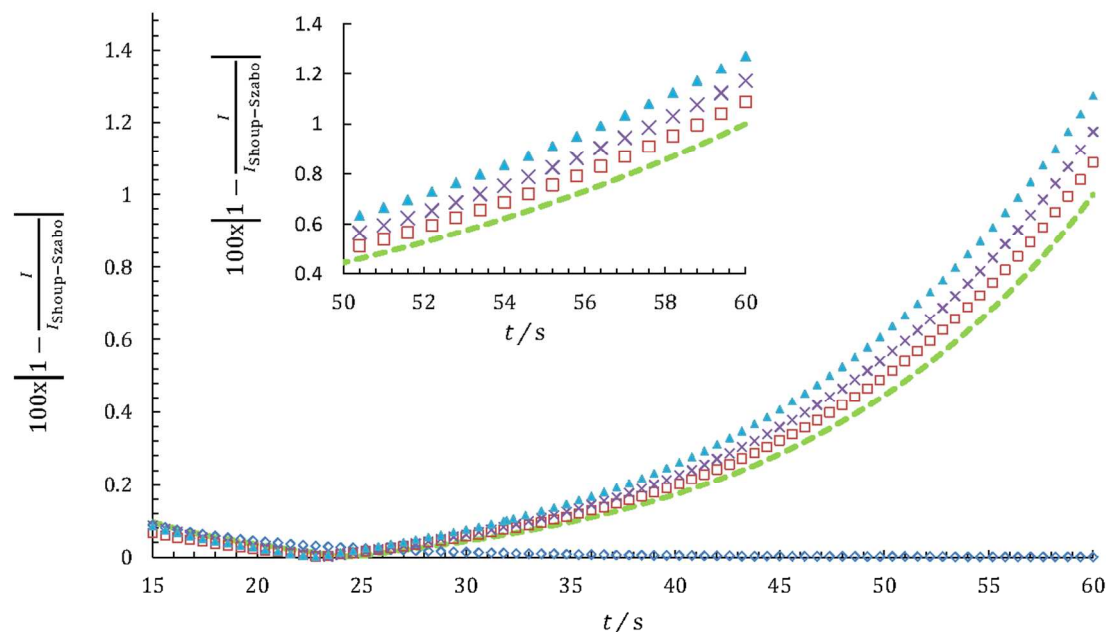


Figure 7. Relative difference between the currents obtained from various simulations and the Shoup-Szabo current (legend as in Figure 2) for an electrode of radius $r_e = 25$ mm. The inset shows the current for the various simulations that involve convection zoomed in for long times. For all simulations, $r_{\max} = z_{\max} = 4r_e = 100$ mm.

Figures 2-7 indicate that, as shown by Ngamchuea et al.², the effect of solutal convection on the chronoamperometric current is appreciable even at an analyte concentration as low as 9.5 mM and timescales as short as 60 s. Just as Ngamchuea et al. observed (consult Table 1 in the paper by Ngamchuea et al.²), the relative difference at $t = t_{\max}$ is largest for millimetre-sized electrodes, ranging from ~ 6 % at $r_e = 0.25$ mm through ~ 12 % for $r_e = 2.5$ mm and diminishing to ~ 1 % at $r_e = 25$ mm. For all setups that included thermal convection, the currents were not distinguishable within the accuracy of the simulations either from each other or from the ones corresponding to just solutal convection.

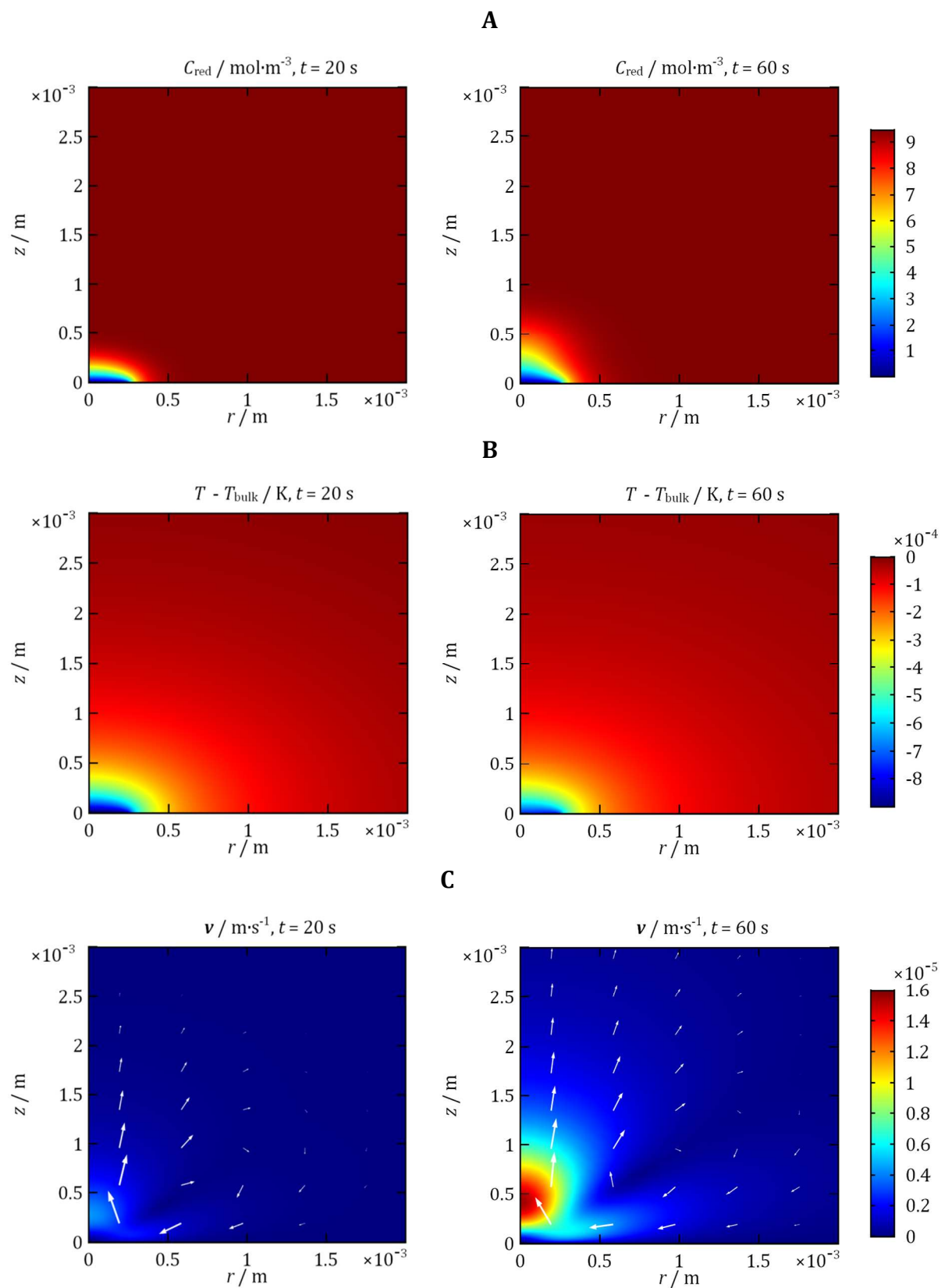


Figure 8. Concentration (A), temperature (B) and velocity profiles (C) at $t = 20$ and 60 s for a chronoamperometric oxidation of $[\text{Fe}(\text{CN})_6]^{4-}$ at an electrode of radius $r_e = 0.25$ mm. The simulations were performed with the experimentally measured enthalpy of the reaction¹², $\Delta H = 45.35$ kJ·mol⁻¹ and a cell of dimensions $r_{\text{max}} = r_e + 6\sqrt{t_{\text{max}}\kappa/(\rho_0 c_p)} = 17.58$ mm by $z_{\text{max}} = 6\sqrt{t_{\text{max}}\kappa/(\rho_0 c_p)} = 17.33$ mm. The length of the arrows representing the velocity vector is proportional to the natural logarithm of $|\mathbf{v}|$.

The results for the concentration and velocity profiles shown in Figures 8-9 are in qualitative agreement with the ones obtained by Ngamchuea et al.² for solutal convection – at short times ($0 < t \sim 20$ s), the absolute value of the velocity is too small ($|\mathbf{v}| \sim 10^{-6}$ m·s⁻¹) to have an appreciable effect on the concentration profile. As time progresses, the product of the reaction accumulates, and the convective flux intensifies, leading to a distorted diffusive boundary layer, whose exact shape depends on the electrode size (see Figures 8A, 9A). The simulated concentration profiles and the measured electrical currents are practically identical for simulations involving only solute-driven convection and those that take thermal convection into account (Figures 2-7, 8A, 9A). The same is observed even in simulations for which the magnitude of the reaction enthalpy was increased and its sign was reversed ($\Delta H = -100$ kJ·mol⁻¹ instead of 45.35 kJ·mol⁻¹). In the latter case, the temperature and velocity profiles are altered (compare Figures 8B-C, 9B-C with Figure S.3B-C and Figure S.8B-C in the Supporting Information), but electrical currents are not appreciably affected (Figures 2-7), even though the thermal and solutal convection act in the same direction.

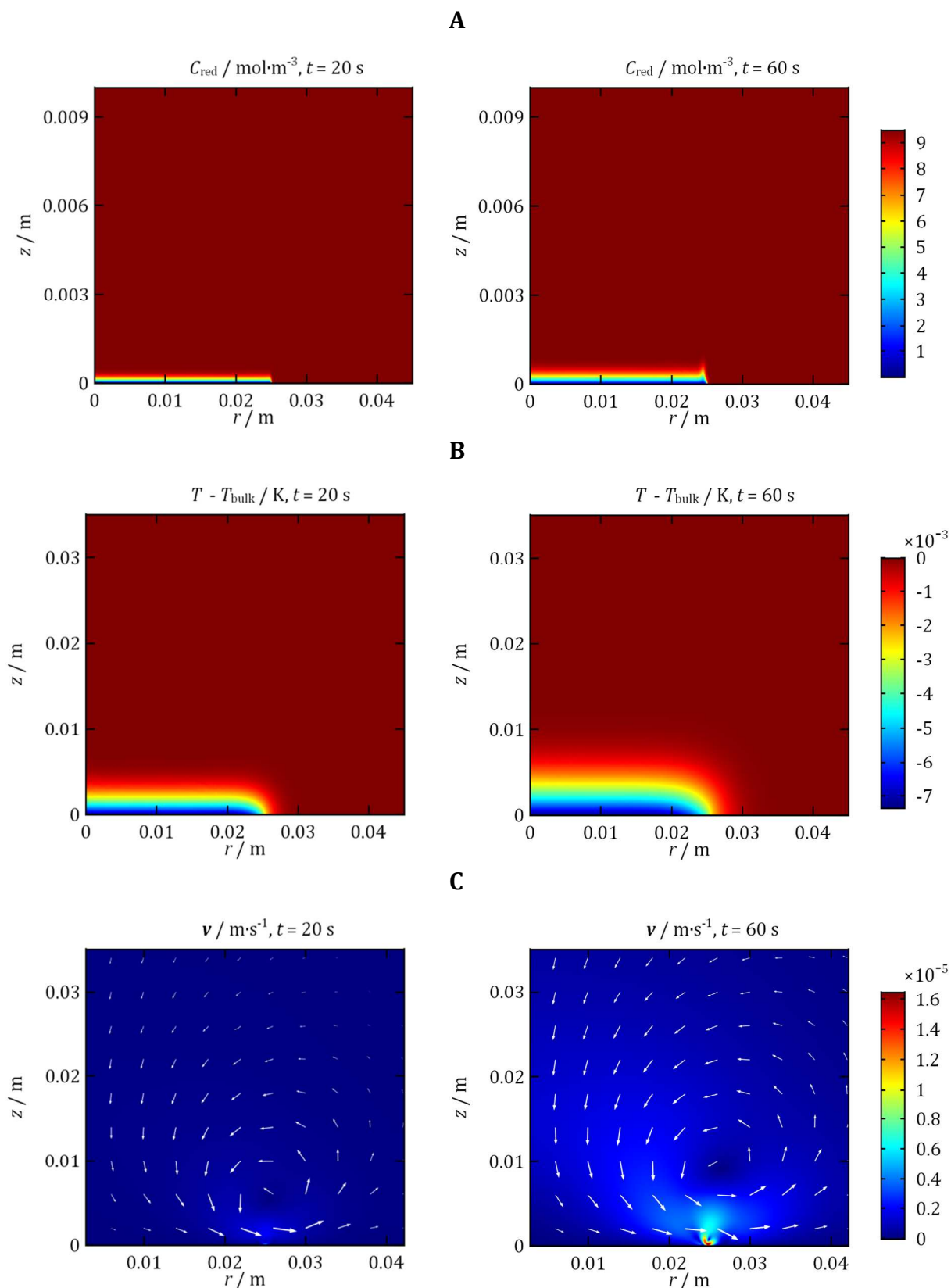


Figure 9. Concentration (A), temperature (B) and velocity profiles (C) at $t = 20$ and 60 s for a chronoamperometric oxidation of $[\text{Fe}(\text{CN}_6)]^{4-}$ at an electrode of radius $r_e = 25 \text{ mm}$. The simulations were performed with the experimentally

measured enthalpy of the reaction¹², $\Delta H = 45.35 \text{ kJ}\cdot\text{mol}^{-1}$ and cell dimensions of , $r_{\text{max}} = z_{\text{max}} = 4r_e = 100 \text{ mm}$. The length of the arrows representing the velocity vector is proportional to the natural logarithm of $|\mathbf{v}|$. Note the different scale of the concentration perturbation (A).

The explanation for this lies in the very low value ($\sim 10^{-3}$) of the buoyancy ratio N (46) for our problem. The numerical estimate for N given in Section II.1 relies on the approximation that the characteristic normal dimensions of the thermal and diffusive boundary layers are of the same order of magnitude as for the convection-free problems, $\sqrt{t\chi}$ and $\sqrt{tD_{\text{red}}}$, respectively. This assumption is supported by the results from our numerical simulations. Using the parameters given below, we can calculate that

$$L_{\text{diff}} = \sqrt{D_{\text{red}}t} = \begin{cases} 1.2 \times 10^{-4} \text{ m}, & t = 20 \text{ s} \\ 1.7 \times 10^{-4} \text{ m}, & t = 40 \text{ s} \\ 2.1 \times 10^{-4} \text{ m}, & t = 60 \text{ s} \end{cases} \quad (51)$$

and

$$L_{\text{therm}} = \sqrt{\chi t} = \begin{cases} 16.7 \times 10^{-4} \text{ m}, & t = 20 \text{ s} \\ 23.6 \times 10^{-4} \text{ m}, & t = 40 \text{ s} \\ 28.9 \times 10^{-4} \text{ m}, & t = 60 \text{ s} \end{cases} \quad (52)$$

On Figures 8-9, we see that the numbers in eqs. (51)-(52) give the correct order of magnitude for the extent of the respective boundary layers in the z -direction, even though the concentration profiles at $t > 40 \text{ s}$ exhibit shapes significantly different from those in the diffusion-only case (compare Figure 8A and Figure 9A with Figure S.1 in the supporting information). It is evident from eq. (46) for the buoyancy ratio, that a change in the orders of magnitude of L_{diff} and L_{therm} would be required to make the effect of thermal convection appreciable.

The compliance of the observed boundary layer thicknesses with eqs. (51)-(52) can be explained via dimensional analysis. The relative importance of convective and diffusive mass transport is quantified by the relevant Péclet number¹¹,

$$Pe_{\text{mass}} = \frac{|\mathbf{v}|r_e}{D_{\text{Red}}}; \quad (53)$$

similarly, the heat transfer Péclet number compares heat transport by convection and conduction¹¹,

$$Pe_{\text{heat}} = \frac{|\mathbf{v}|r_e}{\chi}. \quad (54)$$

The order of magnitude of the flow velocity generated by the electrochemical reaction reaches $|\mathbf{v}| \sim 1.6 \times 10^{-5} \text{ m}\cdot\text{s}^{-1}$ at the end of the simulated experiment for all configurations, see Figures 8-9. Substituting this value for $|\mathbf{v}|$, $r_e = 0.25 \text{ mm}$ and the diffusivities given below, we obtain the assessments $Pe_{\text{mass}} \sim 10$ and $Pe_{\text{heat}} \sim 10^{-2}$ for the

Péclet numbers. This means that, by $t = t_{\max}$, convection becomes the main mode of mass transfer, but heat is still predominantly dissipated via conduction, i.e., the term $\mathbf{v} \cdot \nabla T$ in eq. (13) is negligible and the thermal boundary layer does indeed have a characteristic length of $L_{\text{therm}} = \sqrt{\chi t}$. Even though convection is the main mode of mass transport by the end of the simulations, the small flow velocities generated by the chemical reaction do not change the order of magnitude of L_{diff} . Therefore, eq. (46) gives an accurate assessment of the buoyancy ratio and thermal convection is much less important than solutal convection. Both Pe_{mass} and Pe_{heat} increase with r_e , and at the largest electrode size, $r_e = 25$ mm, we have $Pe_{\text{mass}} \sim 10^3$ and $Pe_{\text{heat}} \sim 1$, i.e., convection plays a significant role in both mass and heat transfer. However, even under those circumstances eqs. (51)-(52) are correct to an order of magnitude (see Figure 9), which means that eq. (46) is approximately valid and thermal convection is still much less important than solutal convection.

However, it is visible from Figures 5 and 7 that the relative significance of thermal convection increases with r_e – while the curves for all simulations involving convection are indistinguishable from one another at $r_e = 0.25$ mm, small differences (within 1 percentage point) are observed between the simulated currents at the larger electrodes. The differences are easily understandable – solutal convection enhances mass transport and leads to a current (squares) that significantly deviates from the one expected in case diffusion is the sole mode of mass transport (solid line). For our model reaction, thermal convection counteracts solute-driven convection (consult eq. (45) and the discussion thereafter), which decreases the current (dashed line), but it still remains considerably higher than the prediction of the Shoup-Szabo equation. By the same token, performing the simulations with a value of the enthalpy change that is reverse in sign leads to a current higher than that obtained from the case with solutal convection only (triangles and crosses), and the magnitude of the effect depends on the absolute value of ΔH . The differences observed on Figures 5 and 7 are subtle and it would be difficult to separate their role from that of external factors typically present in electrochemical experiments, e.g. vibrations²⁹. Moreover, as they are smaller than the error of the diffusion only simulations (diamonds on Figures 2-7), their interpretation should be done with care.

While these conclusions are valid for all the configurations studied here, they do not necessarily apply to all circumstances – at sufficiently long times and sufficiently large electrodes, thermal and solutal convection may become comparable and the interplay between them will be more complex. This case, however, goes beyond the scope of our study, which is concerned with typical experimental conditions encountered in electroanalysis.

2. Cyclic Voltammetry

The simulated voltammetric currents for all simulations described in Section II.2 are plotted in Figures 10-12. The profiles of C_{red} , v and T for the studied cases are given in Section S.2 of the Supporting Information.

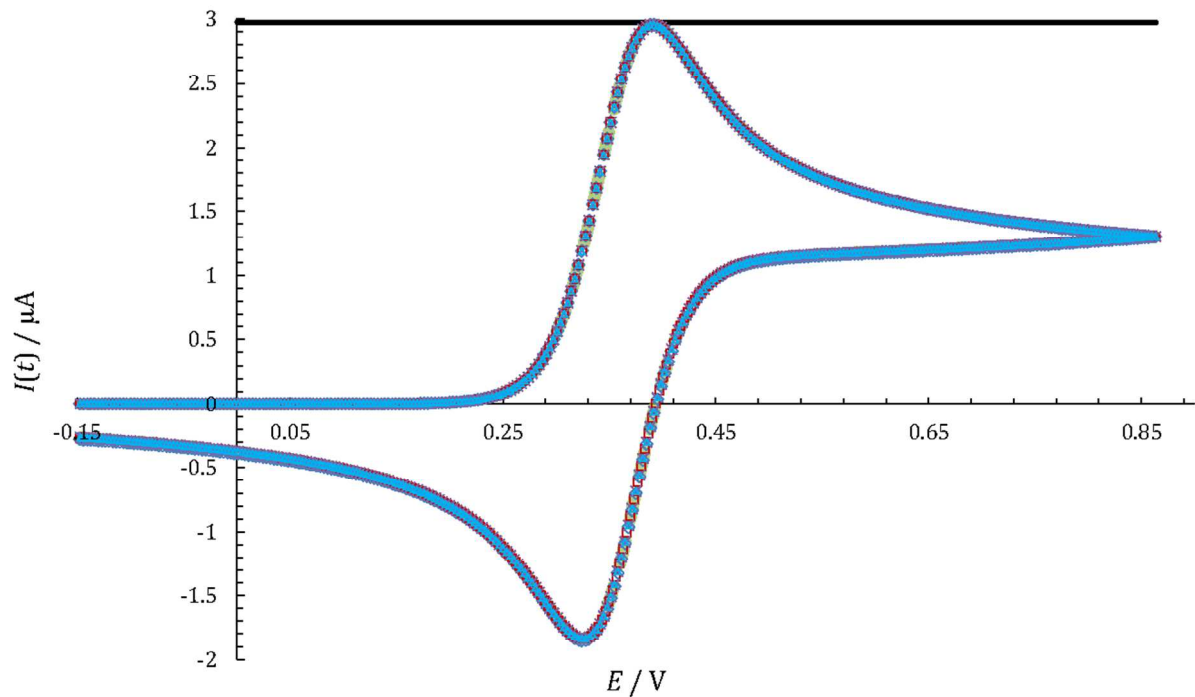


Figure 10. Cyclic voltammogram for $r_e = 0.25$ mm at a scan rate of $33.7 \text{ mV}\cdot\text{s}^{-1}$. Legend as follows: solid line –theoretical peak for the diffusion-only case (eq. (49)); diamonds - diffusion-only simulation; squares – simulation with convection driven by concentration gradients; dashed line – simulation with convection driven by concentration and temperature gradients with $\Delta H = 45.35 \text{ kJ}\cdot\text{mol}^{-1}$; crosses – simulation with convection driven by concentration and temperature gradients with $\Delta H = -45.35 \text{ kJ}\cdot\text{mol}^{-1}$; triangles – simulation with convection driven by concentration and temperature gradients with $\Delta H = -100.0 \text{ kJ}\cdot\text{mol}^{-1}$. The simulations were performed with $r_{\text{max}} = r_e + 6\sqrt{t_{\text{max}}\kappa/(\rho_0 c_p)} = 17.58 \text{ mm}$, $z_{\text{max}} = 6\sqrt{t_{\text{max}}\kappa/(\rho_0 c_p)} = 17.33 \text{ mm}$.

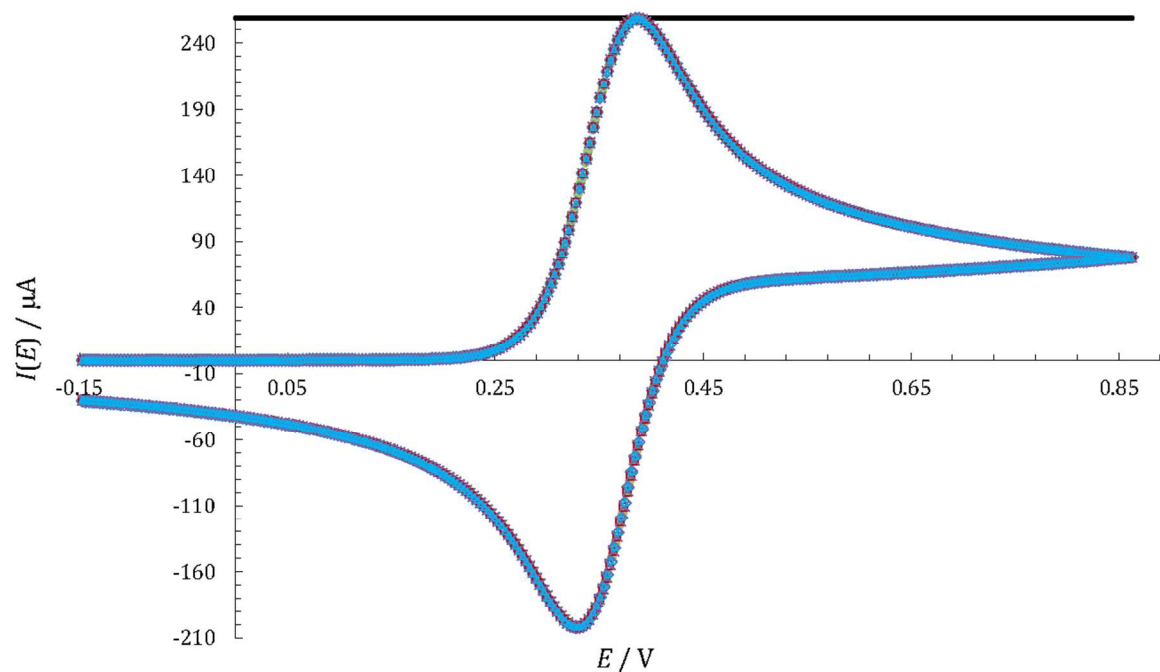


Figure 11. Cyclic voltammogram for $r_e = 2.5$ mm at a scan rate of $33.7 \text{ mV}\cdot\text{s}^{-1}$. Legend as in Figure 10. The simulations were performed with $r_{\text{max}} = r_e + 6\sqrt{t_{\text{max}}\kappa/(\rho_0 c_p)} = 19.82$ mm, $z_{\text{max}} = 6\sqrt{t_{\text{max}}\kappa/(\rho_0 c_p)} = 17.3$ mm.

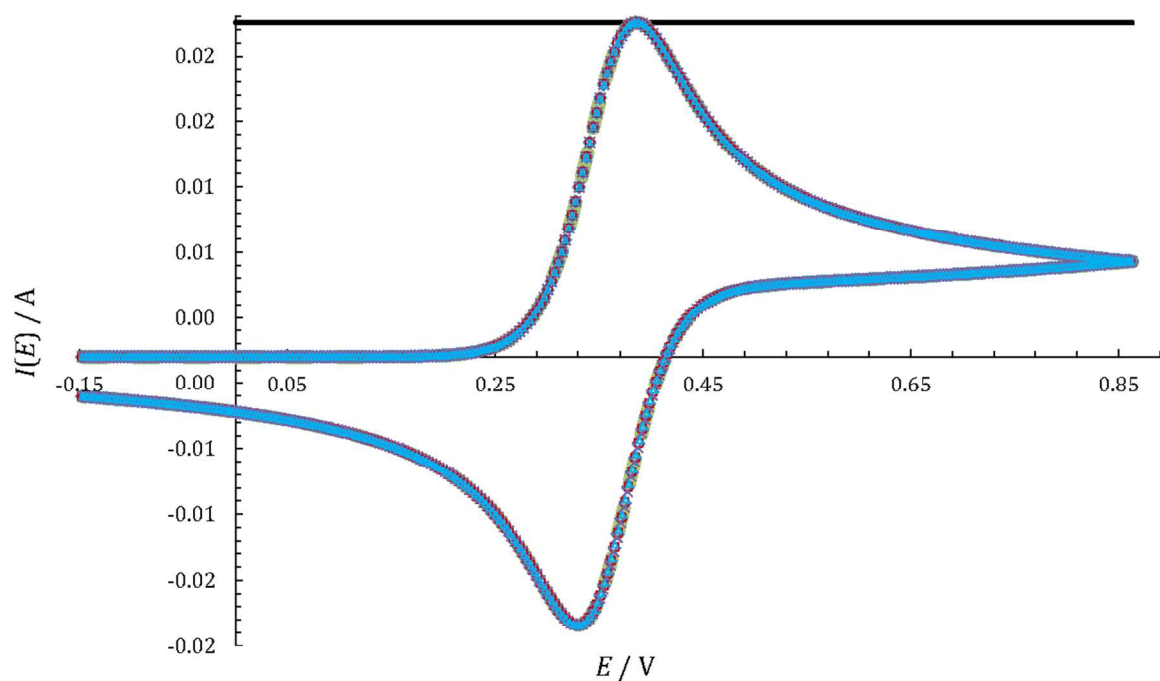


Figure 12. Cyclic voltammogram for $r_e = 25$ mm at a scan rate of $33.7 \text{ mV}\cdot\text{s}^{-1}$. Legend as in Figure 10. The simulations were performed with $r_{\text{max}} = z_{\text{max}} = 0.1$ m.

The heights of the forward and backward peak were used as criteria for the relative differences between them. Within the precision of our simulations, these two

characteristics are indistinguishable from their values for the convection-free case. Thus, in contrast with chronoamperometry, under the studied conditions cyclic voltammetry is unaffected by either solutal or thermal convection. The reason for this qualitative difference is that the potential is varied continuously (eq. (50)) between a value at which no reaction occurs and the potential applied in chronoamperometry ($E_v = E_{\text{chrono}}$) that ensures that upon reaching the electrode surface, the reactant is practically completely converted to product (see eq. (9)). As the scan rate in our simulations is chosen in such a way that the duration of the scan (t_{max}) is equal to that of the chronoamperometric oxidation, this means that reaction (1) occurs over a much shorter time period in cyclic voltammetry than in chronoamperometry. Consequently, the build-up of product that drives the solutal convection is much less pronounced. Furthermore, the cumulative effect in chronoamperometry resulting from the build-up of product over the course of the whole process is reversed in the second half of the potential scan. Though the simulated electrical currents are unaffected by the presence of convection, the same is not true for the concentration profiles (see Section S.2 of the Supporting Information) and it is possible for convective flows to become important under different conditions, e.g., a lower scan rate and/or a longer duration of the scan.

IV. Conclusions

In this paper, we have investigated the effect of natural convection driven by gradients in temperature and solute concentration on the currents measured in the important electroanalytical techniques chronoamperometry and cyclic voltammetry. We have performed numerical simulations of the electrochemical oxidation of hexacyanoferrate (II) to hexacyanoferrate (III) at a range of electrode sizes.

In agreement with the results reported in a recent study by Ngamchuea et al.², we see that if the model reaction occurs under chronoamperometric conditions, solutal convection leads to a significantly higher electrical current than the one predicted by the Shoup-Szabo equation for the diffusion-only case due to the enhanced mass transport (Figures 2-7). Even though thermal convective flows are always generated by the change of enthalpy associated with the electrochemical reaction, our results indicate that their role is negligible for all cases considered here. The explanation behind this lies in the different length scales over which the perturbations in temperature and concentration spread. As heat propagates through the solution much faster than mass, the characteristic length of the thermal boundary layer is much larger than that of the diffusion boundary layer, which results in a negligible contribution of the variations in temperature to the buoyancy force, see eq. (45) above. This assertion is confirmed by the results from our simulations at all considered electrode sizes (ranging from 0.25 to 25 mm). Even when the enthalpy change was set to a value several times greater in absolute value and reverse in sign ($\Delta H = -100.0$

kJ·mol⁻¹ instead of 45.35 kJ·mol⁻¹), the effect of thermal convection on the electrical current was within the numerical accuracy of the simulations.

Remarkably, our simulations show that neither solute-driven nor thermal convection exerts an appreciable influence on the electrical current measured in cyclic voltammetry. As discussed in Section III.2, this is due to the shorter timescale over which the model reaction occurs and the occurrence of the reverse reaction during the second half of the scan.

To summarize, the main finding of the hereby presented work is that thermal convection has a negligible effect on the currents measured in both chronoamperometry and cyclic voltammetry. Our work provides important physical insight into an effect that has received little attention in the literature despite its ubiquity, thereby furthering the understanding of the studied electroanalytical techniques. A future development of the topic would be a study of the effect of natural convection on measurements made with SECM. Having in mind the results presented here, we do not expect reaction-induced thermal convection to be important in this case.

Supporting Information. Plots of the concentration, temperature and velocity profiles for the simulations described in II.2 are given in the Supporting Information.

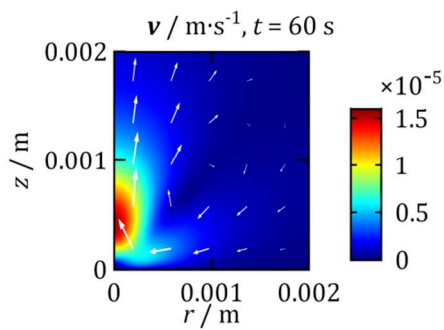
Acknowledgements. We thank Dr. Enno Kätelhön for helpful discussions. J.K.N thanks the Clarendon Fund and Trinity College of the University of Oxford for financial support. Shaltiel Eloul has received funding from the European Research Council under the European Union's Seventh Framework Programme (FP/2007-2013) / ERC Grant Agreement n. [320403].

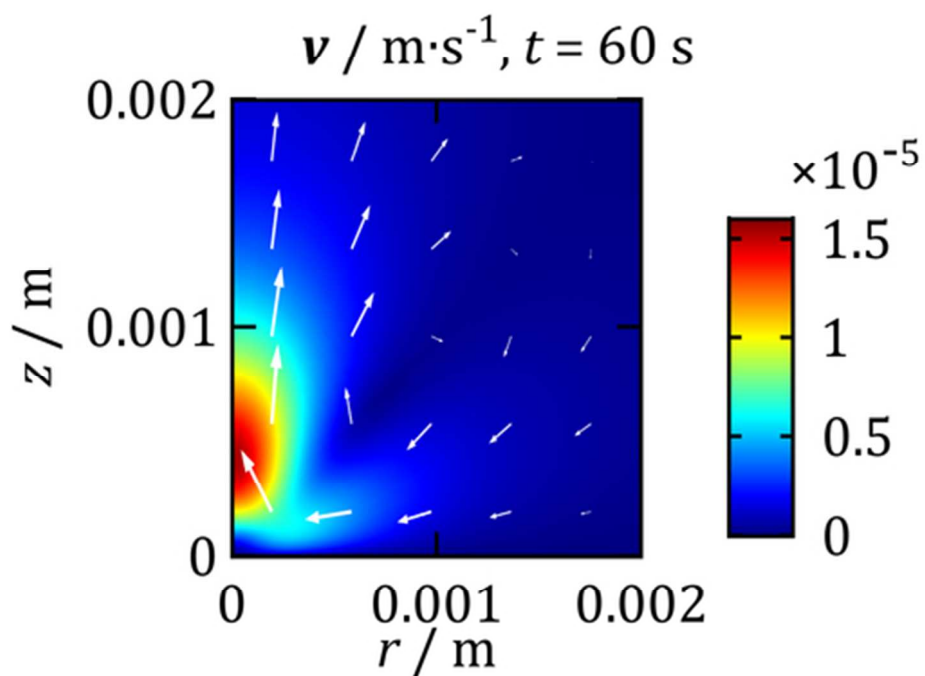
References

1. Sahore, V.; Kreidermacher, A.; Khan, F.Z.; Fritsch, I. Visualization and Measurement of Natural Convection from Electrochemically-Generated Density Gradients at Concentric Microdisk and Ring Electrodes in a Microfluidic System. *J. Electrochem Soc.* **2016**, *163*, H3135-H3144.
2. Ngamchuea, K.; Eloul, S.; Tschulik, K.; Compton, R.G. Advancing from Rules of Thumb: Quantifying the Effects of Small Density Changes in Mass Transport to Electrodes. Understanding Natural Convection. *Anal. Chem.* **2015**, *87*, 7226-7234.
3. Padova, J. Ion—Solvent Interaction. II. Partial Molar Volume and Electrostriction: a Thermodynamic Approach. *J. Chem. Phys.* **1963**, *39*, 1552-1557.

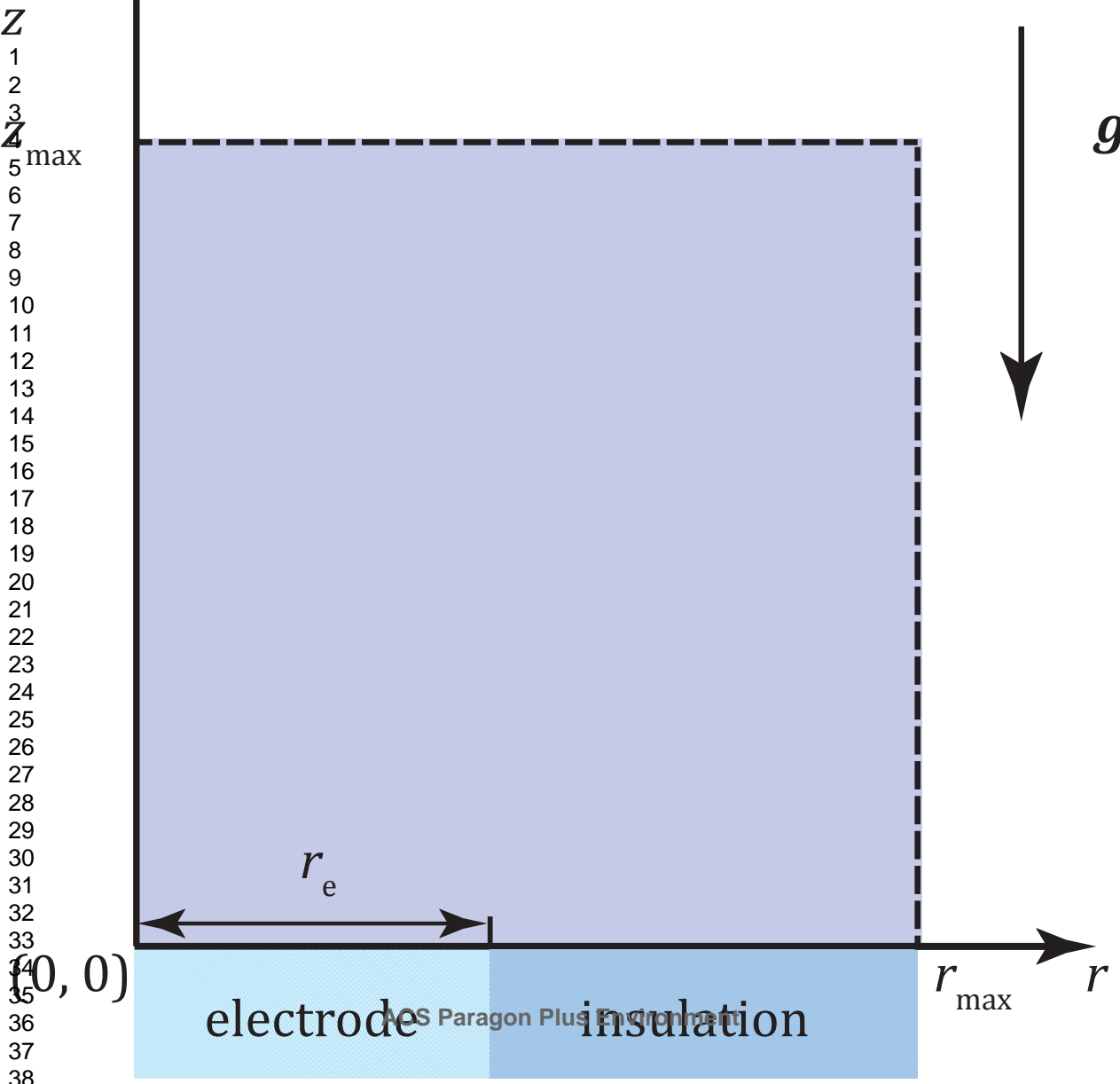
4. Selman, J.R.; Newman, J. Free-Convection Mass Transfer with a Supporting Electrolyte. *J. Electrochem. Soc.* **1971**, *118*, 1070-1078.
5. Bond, A.M.; Coomber, D.C.; Feldberg, S.W.; Oldham, K.B.; Vu, T. An Experimental Evaluation of Cyclic Voltammetry of Multicharged Species at Macrodisk Electrodes in the Absence of Added Supporting Electrolyte. *Anal. Chem.* **2001**, *73*, 352-359.
6. Gao, X.; Lee, J.; White, H.S. Natural Convection at Microelectrodes. *Anal. Chem.* **1995**, *67*, 1541-1545.
7. Beckmann, A.; Coles, B.A.; Compton, R.G.; Gründler, P.; Marken, F.; Neudeck, A. Modeling Hot Wire Electrochemistry. Coupled Heat and Mass Transport at a Directly and Continuously Heated Wire. *J. Phys. Chem. B* **2000**, *104*, 764-769.
8. Kamotani, Y.; Wang, L.W.; Ostrach, S.; Jiang, H.D. Experimental Study of Natural Convection in Shallow Enclosures with Horizontal Temperature and Concentration Gradients. *Int. J. Heat Mass Transfer* **1985**, *28*, 165-173.
9. Compton, R.G.; Laborda, E.; Ward, K. R. *Understanding Voltammetry: Simulation of Electrode Processes*; Imperial College Press: London, 2014.
10. Dickinson, E.J.F.; Limon-Petersen, J.G.; Rees, N.V.; Compton, R.G. How Much Supporting Electrolyte Is Required to Make a Cyclic Voltammetry Experiment Quantitatively "Diffusional"? A Theoretical and Experimental Investigation. *J. Phys. Chem. C* **2009**, *113*, 11157-11171.
11. Bird, R. B.; Stewart, W.E.; Lightfoot, E.N. *Transport Phenomena*, 2nd Edition; Wiley: New York, 2002.
12. Boudeville, P.; Tallec, A. Electrochemistry and Calorimetry Coupling. IV. Determination of Electrochemical Peltier Heat. *Thermochim. Acta* **1988**, *126*, 221-234.
13. Ozeki, T.; Ogawa, N.; Aikawa, K.; Watanabe, I.; Ikeda, S. Thermal Analysis of Electrochemical Reactions: Influence of Electrolytes on Peltier Heat for Cu(0)/Cu(II) and Ag(0)/Ag(I) Redox Systems. *J. Electroanal. Chem.* **1983**, *145*, 53-65.
14. Fang, Z.; Wang, S.; Zhang, Z. The Peltier Heat and the Standard Electrode Potential of Ferro-ferricyanide Couple at 298.15 K Determined by Electrochemical-Calorimetry. *J. Therm. Anal. Calorim.* **2011**, *106*, 937-943.
15. Demkowicz, L. A Note on Symmetry Boundary Conditions in Finite Element Methods. *Appl. Math. Lett.* **1991**, *4*, 27-30.
16. Harned, H.S.; Owen, B.B. *The Physical Chemistry of Electrolytic Solutions*; Reinhold: New York, 1958.
17. Feldberg, S. W.; Lewis, E.R. Concentration and Density Changes at an Electrode Surface and the Principle of Unchanging Total Concentration. *J. Electrochem. Soc.* **2016**, *163*, H3167-H3172.
18. Marcus, Y. *Ion Properties*; Marcel Dekker: New York, 1997.
19. Landau, L.D; Lifschitz, E.M. *Fluid Mechanics*, 2nd Edition; Pergamon Press: Oxford, 1987.

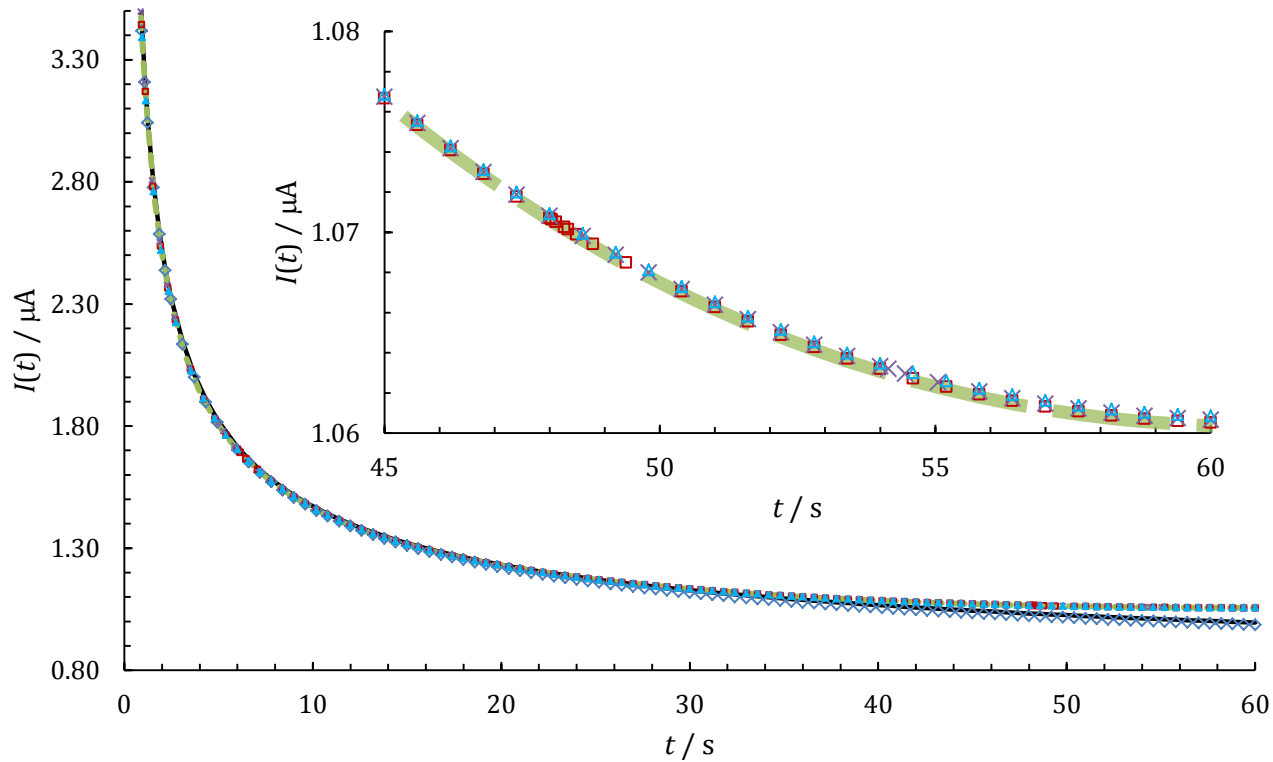
20. Vetter, K.J. *Electrochemical Kinetics: Theoretical Aspects*; Academic Press: New York, 1967.
21. Pringle, S.E.; Glass, R.J. Double-diffusive Finger Convection: Influence of Concentration at Fixed Buoyancy Ratio. *J. Fluid Mech.* **2002**, *462*, 161-183.
22. Singh, O.P.; Srinivasan, J. Effect of Rayleigh numbers on the Evolution of Double-diffusive Salt Fingers. *Phys. Fluids* **2014**, *26*, 062104-1–062104-18.
23. Lide, D.R., Ed., *CRC Handbook of Chemistry and Physics*, Internet Version 2005; CRC Press: Boca Raton, FL, 2005.
24. Dickinson, E.J.F.; Ekström, H.; Fontes, E. COMSOL Multiphysics®: Finite Element Software for Electrochemical Analysis. A Mini-review. *Electrochem. Commun.* **2014**, *40*, 71-74.
25. Ngamchuea, K.; Eloul, S.; Tschulik, K.; Compton, R.G. Planar Diffusion to Macro Disc Electrodes—What Electrode Size Is Required for the Cottrell and Randles-Sevcik Equations to Apply Quantitatively? *J. Solid State Electrochem.* **2014**, *18*, 3251-3257.
26. Gray, D.D.; Giorgini, A. The Validity of the Boussinesq Approximation for Liquids and Gases. *Int. J. Heat Mass Transfer* **1976**, *19*, 545-551.
27. Shoup, D.; Szabo, A. Chronoamperometric Current at Finite Disc Electrodes. *J. Electroanal. Chem.* **1982**, *140*, 237-245.
28. Compton, R.G.; Banks, C.E. *Understanding Voltammetry*, 2nd Edition; Imperial College Press: London, 2011.
29. Amatore, C.; Szunerits, S.; Thouin, L.; Warkocz, J.-S. The Real Meaning of Nernst's Steady Diffusion Layer Concept under Non-forced Hydrodynamic Conditions. A Simple Model Based on Levich's Seminal View of Convection. *J. Electroanal. Chem.* **2001**, *500*, 62-70.

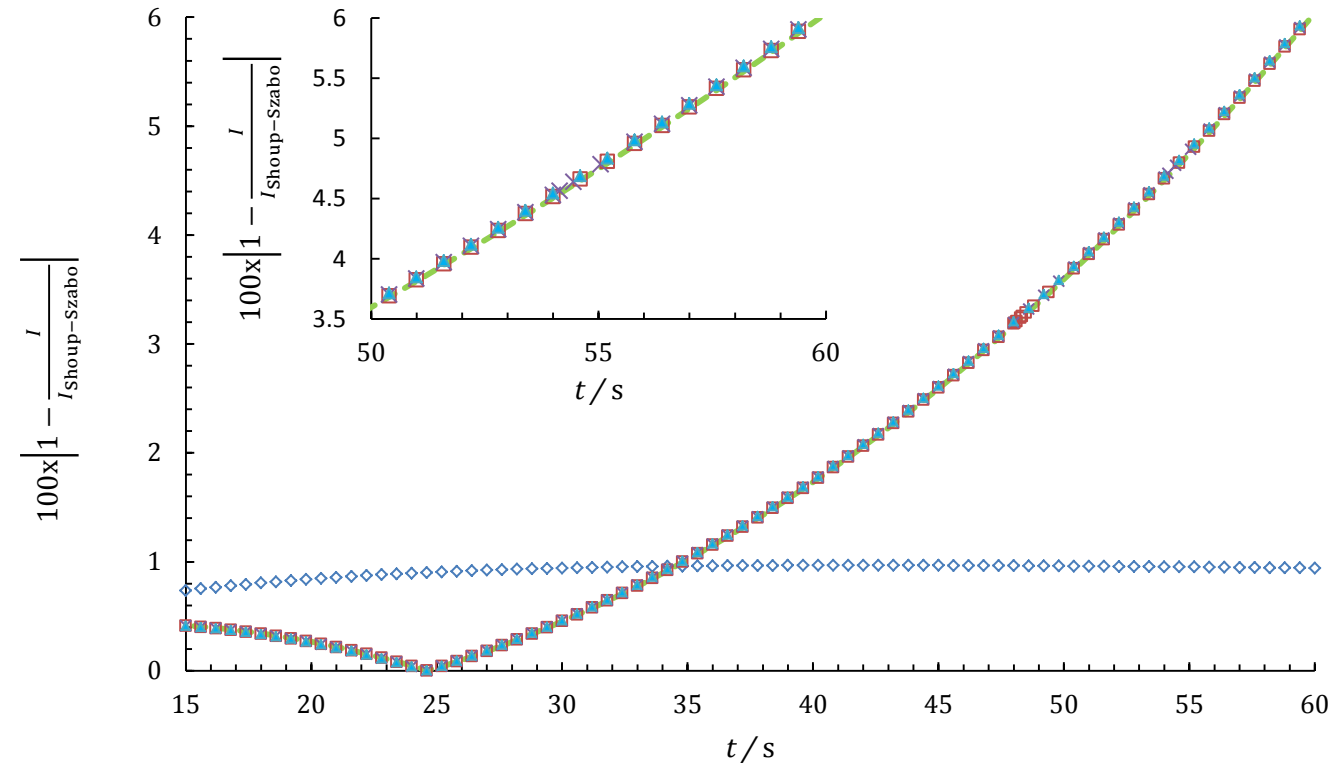


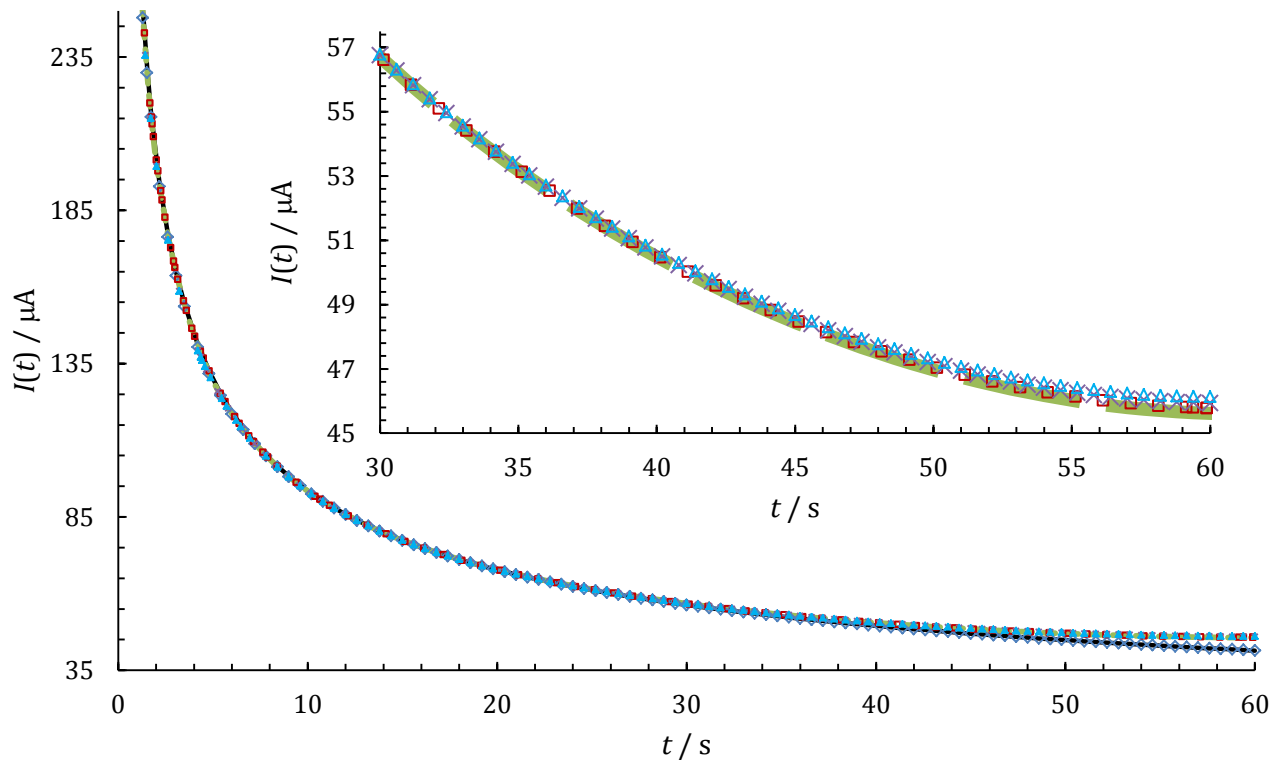


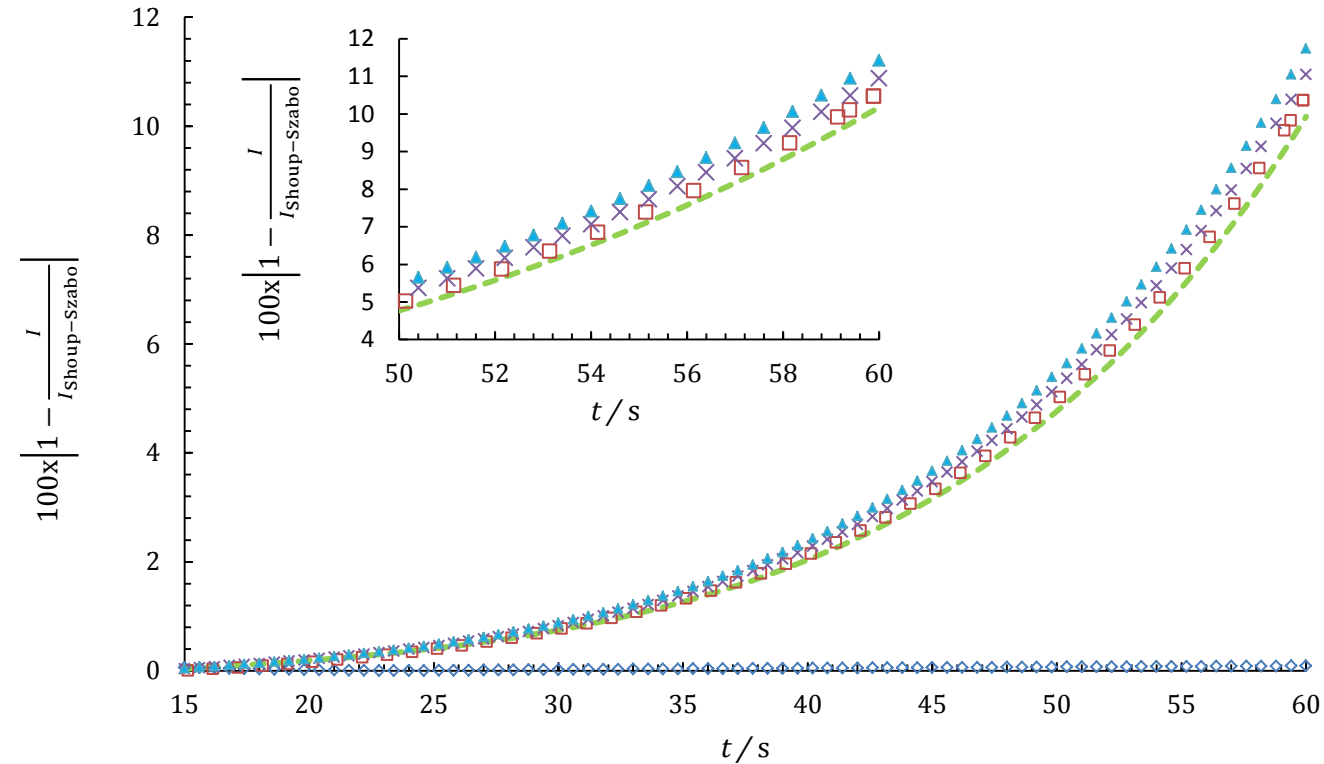
46x35mm (300 x 300 DPI)

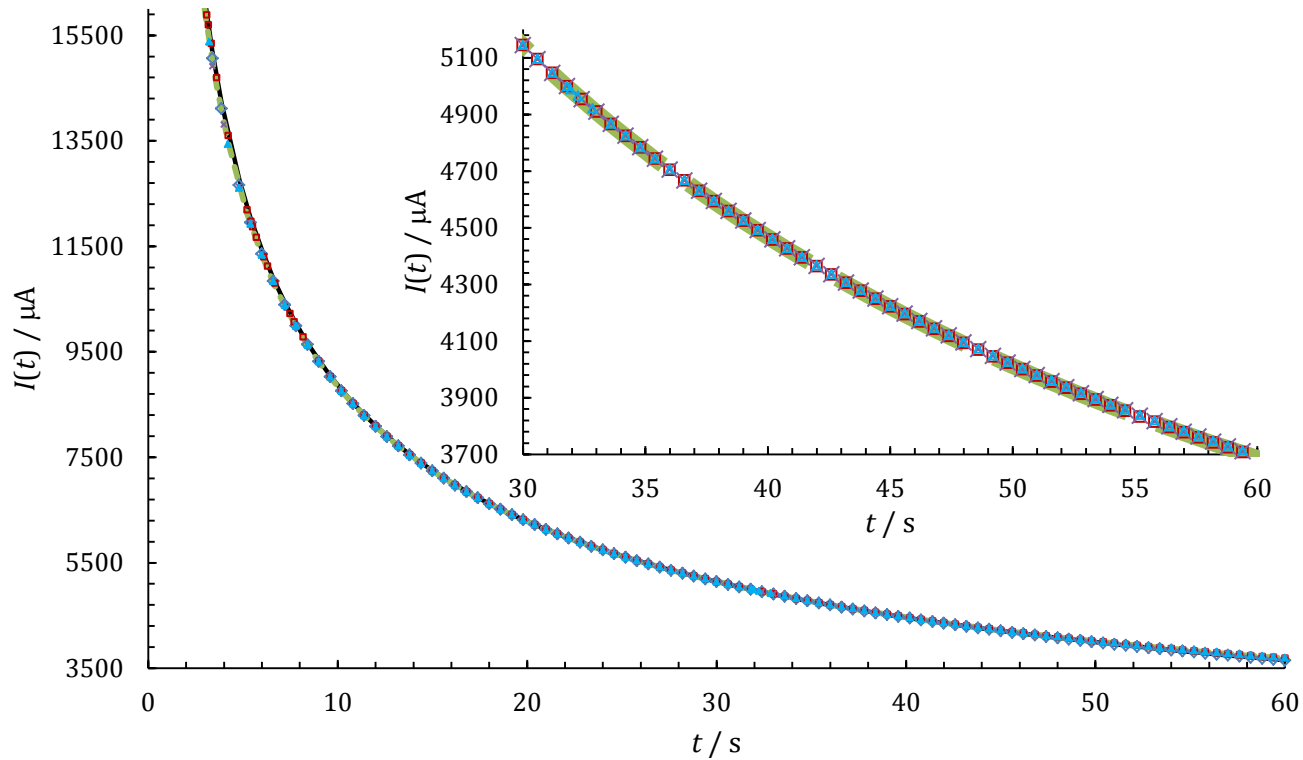


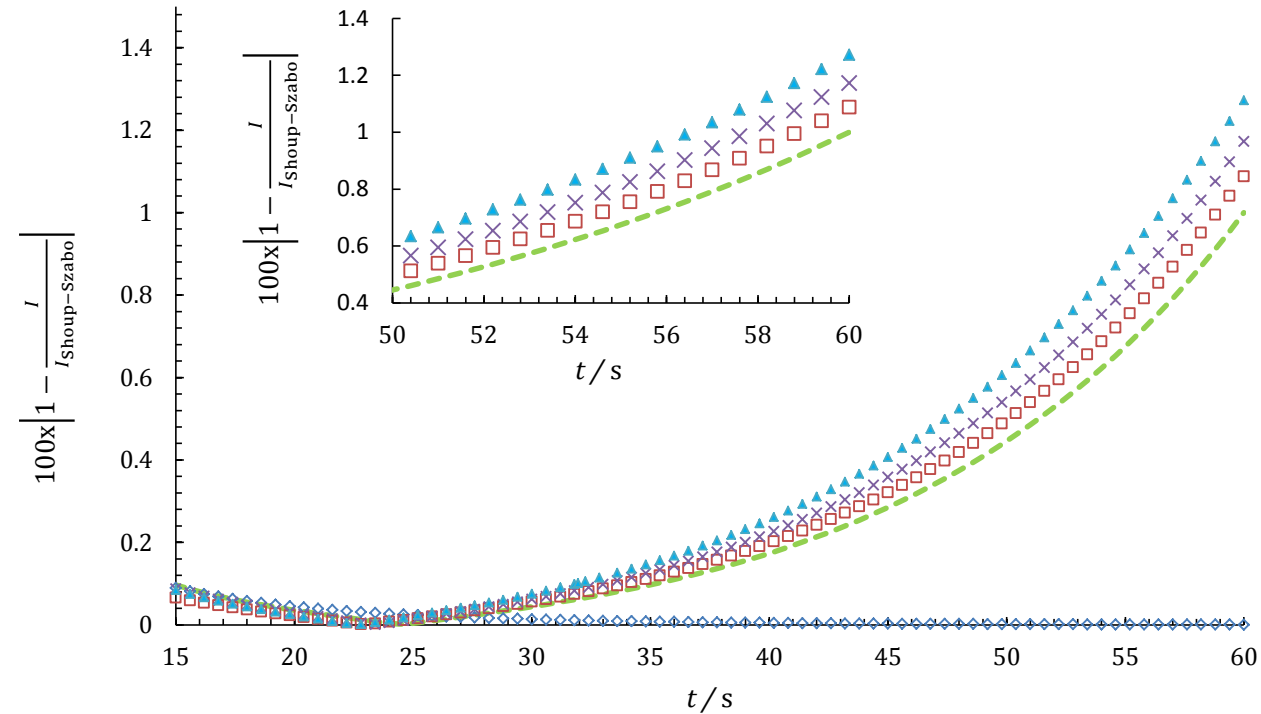


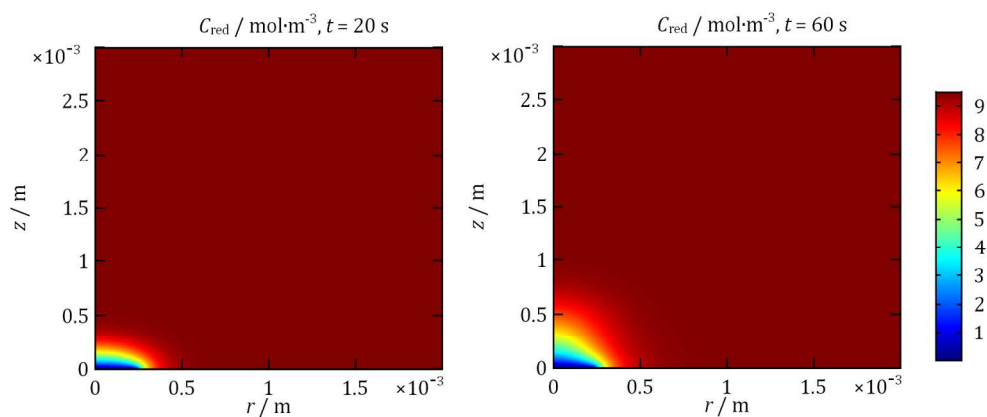




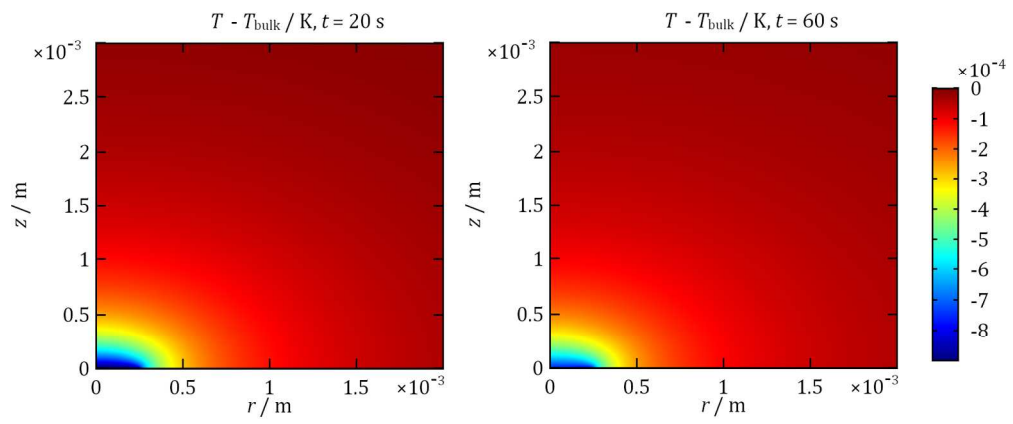




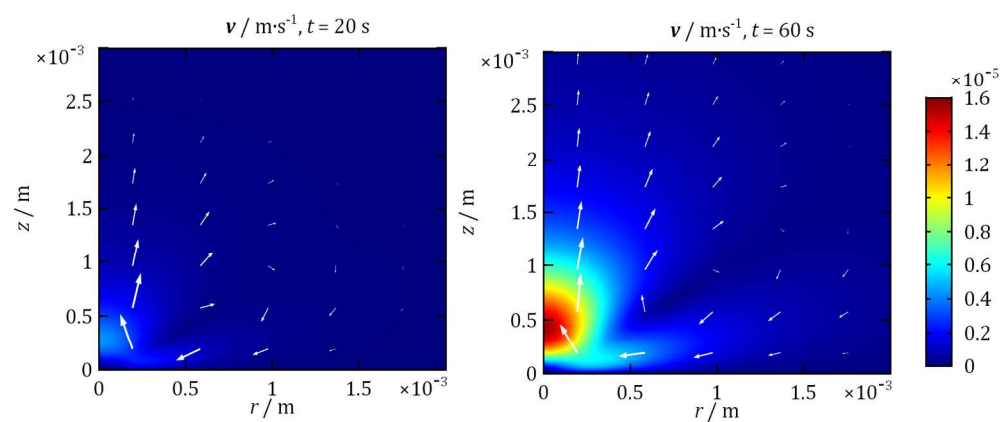




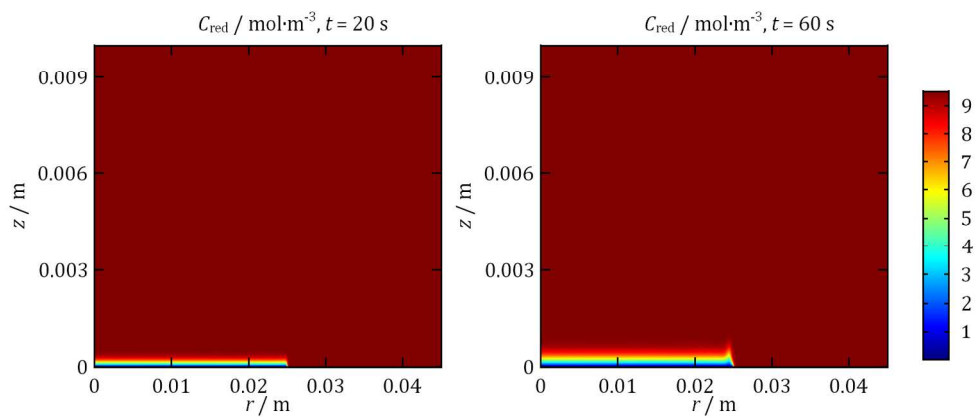
155x67mm (300 x 300 DPI)



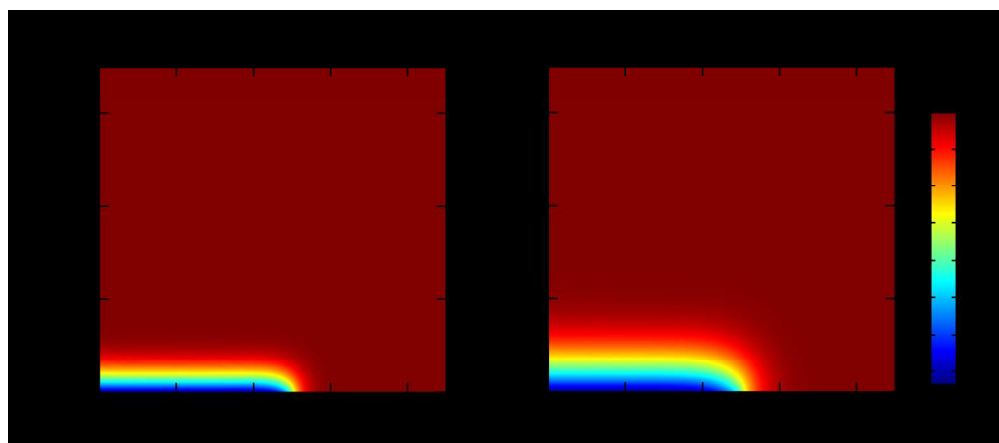
155x67mm (300 x 300 DPI)



155x67mm (300 x 300 DPI)

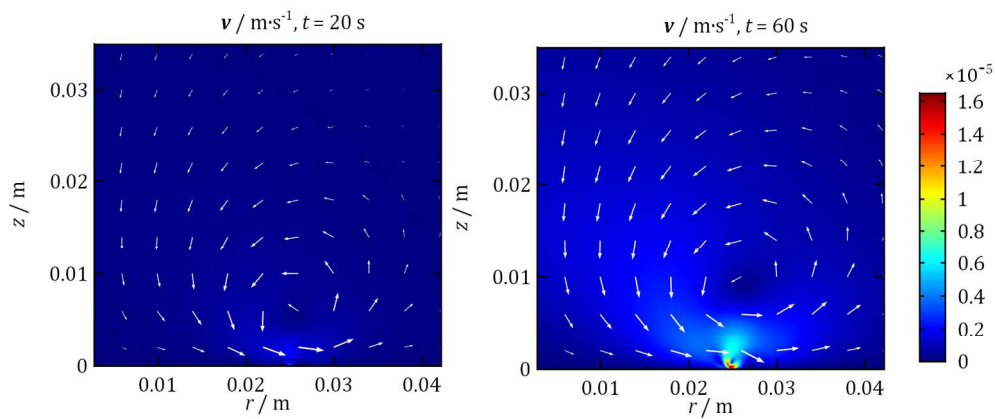


155x67mm (300 x 300 DPI)



155x67mm (300 x 300 DPI)

1
2
3
4
5
6
7
8
9
10
11
12
13
14
15
16
17
18
19
20
21
22
23
24
25
26
27
28
29
30
31
32
33
34
35
36
37
38
39
40
41
42
43
44
45
46
47
48
49
50
51
52
53
54
55
56
57
58
59
60



155x67mm (300 x 300 DPI)

